THESIS FOR THE DEGREE OF DOCTOR OF PHILOSOPHY

High resolution microstructural characterization of oxide thin films and interfaces

NIKOLINA TUZLA

Department of Applied Physics
CHALMERS UNIVERSITY OF TECHNOLOGY
Göteborg, Sweden 2013

High resolution microstructural characterization of oxide thin films and interfaces

Nikolina Tuzla

© Nikolina Tuzla, 2013.

ISBN 978-91-7385-915-8
Doktorsavhandlingar vid Chalmers tekniska högskola
Ny serie nr 3596
ISSN 0346-718X

Department of Applied Physics
Chalmers University of Technology
SE-412 96 Göteborg
Sweden
Telephone + 46 (0) 31-772 1000

Cover: The lower left figure, a HAADF STEM image acquired in a C_s corrected Titan TEM, showing $LaAlO_3/SrTiO_3$, oxide heterostructure, with a transparent red line through the interface, illustrating region of the 2DEG . Figure to the right is a high resolution transmission electron microscopy (HRTEM) view of the Yttrium stabilized Zirconium thin film on top of the $SrTiO_3$ substrate. Schematic models to the right in each hexagon are illustrating simple models of the corresponding cubic oxide material unit cells.

Chalmers Reproservice
Göteborg, Sweden 2013

High resolution microstructural characterization of oxide thin films and interfaces

Nikolina Tuzla
Department of Applied Physics
Chalmers University of Technology

Abstract

Oxide interfaces can introduce properties that are different compared to the corresponding crystal bulk properties. The properties can be tuned by changing the structure. It has become clear that these oxide interface systems are potentially suitable for future electronic devices with unique and tailored properties. The fine scale structure of the interfaces affects the properties and enables the control of them provided that a knowledge about the correlation between structure and properties has been established. In this thesis work, the microstructure of oxide interfaces has been correlated to the electrical transport properties mainly by imaging and spectroscopy using transmission electron microscopy.

$SrTiO_3$ (STO) and $LaAlO_3$ (LAO) are well-studied dielectric materials with wide band gaps of about 3.2 and 5.6 eV respectively. A highly conducting layer forms at the interface between thin films of these insulators under certain circumstances. The induced electrical conductivity is proposed to be due to oxygen vacancies, intermixing and/or a polar discontinuity at the LAO/STO interface. In order to further clarify the mechanisms that occur at the interfaces, details about the atomic structure at interfaces between LAO and (001) STO have been studied by atomic number contrast in HAADF STEM.

In addition to the perovskite oxide systems, also the combined fluorite/perovskite heterostructures have attracted interest. There is a need to increase understanding for the electrical transport properties in heterostructures between large misfit structures. These nanostructured systems have already showed potential to be used in solid oxide fuel cells (SOFC) as well as gas sensors. Bulk Yttrium stabilized Zirconium (YSZ) is a widely used ionic conductor material at elevated temperatures in solid electrolytes in solid oxide fuel cells. In this work, the microstructure of thin films of YSZ on top of STO and LAO substrates have been investigated. We show important changes in the film orientation and morphology as a function of substrate and deposition temperature.

The techniques used in this thesis work include high angle annular dark field scanning transmission electron microscopy (HAADF STEM), high resolution transmission electron microscopy (HRTEM), electron diffraction, energy dispersive X-ray spectroscopy (EDS), x-ray diffraction (XRD), medium energy ion spectroscopy

(MEIS) and atomic force microscopy (AFM). The oxide interfaces were introduced in thin films deposited using the pulsed laser deposition technique.

Keywords: Microstructure, interfaces, oxides, heterostructures, thin films, TEM, HAADF STEM, $SrTiO_3$, $LaAlO_3$, 2DEG, YSZ.

PREFACE

The research presented in this doctoral thesis has been carried out at the Microscopy and Microanalysis group and at the Eva Olsson Group at the Department of Applied Physics, Chalmers University of Technology, Göteborg, Sweden, 2008 to 2013, under the supervision of Prof. Eva Olsson. This work has been a part of collaboration with Ass. Prof Alexey Kalabukhov, Pier Paolo Aurino, Prof. Dag Winkler and Prof. Tord Claeson at the Quantum Device Physics Laboratory, Department of Microelectronics and Nanoscience. Part of the work has been performed in collaboration with Prof. Ariando and collaborators, NUSNNI-Nanocore and Department of Physics, National University of Singapore, Singapore.

List of Appended Papers

I. P.P. Aurino, A. Kalabukhov, N.Tuzla, E. Olsson, T. Claeson and D. Winkler, *"Nanopatterning of the electron gas at the $LaAlO_3/SrTiO_3$ interface using low-energy ion beam irradiation"* Appl. Phys. Lett. **102**, 201610 (2013).

II. N. Tuzla, P.P. Aurino, A. Kalabukhov, T. Claeson, D. Winkler and E. Olsson, *"Microstructural characterization of the Ar+ion irradiation effect on the electron gas at the patterned $LaAlO_3/SrTiO_3$ interface",* in manuscript.

III. A. Annadi, Q. Zhang, X. Renshaw Wang, N. Tuzla, K. Gopinadhan, W.M. Lu , A. Roy Barman, Z.Q. Liu, A. Srivastava, S. Saha, Y.L. Zhao, S.W. Zeng, S. Dhar, E. Olsson, B. Gu, S. Yunoki, S. Maekawa, H. Hilgenkamp, T. Venkatesan and Ariando, *"Anisotropic two-dimensional electron gas at the $LaAlO_3/SrTiO_3$ (110) interface",* Nature Communications **4**, 1838 (2013).

IV. N. Tuzla, A.E. Zaghi, A.S. Kalabukhov, D. Winkler and E. Olsson, *"Controlling surface topography and texture of YSZ films on $SrTiO_3$ substrates by oxygen pressure during deposition*", in manuscript.

V. N. Tuzla, A.E. Zaghi, A.S. Kalabukhov, D. Winkler and E. Olsson, *"Difference in crystallographic texture and microstructure of YSZ films on $SrTiO_3$ and $LaAlO_3$ substrates*", in manuscript.

Specification of My Contribution to the Included Papers

My contributions to the included papers were as follows:

I. I did the TEM work and co-wrote the paper

II. I did the TEM work, all data analysis and wrote the paper

III. I did the TEM work and co-wrote the TEM related part

IV. I did the TEM work, all data analysis and wrote the paper

V. I did the TEM work, all data analysis and wrote the paper

Related Papers

A. A. Kalabukhov, Yu. A. Boikov, I. T. Serenkov, V. I. Sakharov, V. N. Popok, R. Gunnarsson, J. Börjesson, N. Ljustina, E. Olsson, D. Winkler and T. Claeson, *"Cationic Disorder and Phase Segregation in $LaAlO_3/SrTiO_3$ Heterointerfaces Evidenced by Medium-Energy Ion Spectroscopy"*, Physical Review Letters **103**(14): 146101 (2009)

B. A. Kalabukhov, Y. A. Boikov, I. T. Serenkov, V. I. Sakharov, J. Börjesson, N. Ljustina, E. Olsson, D. Winkler and T. Claeson, *"Improved cationic stoichiometry and insulating behavior at the interface of LaAlO3/SrTiO3 formed at high oxygen pressure during pulsed-laser deposition"*, EPL **93**, 37001 (2011)

C. A. Kalabukhov, T. Claeson, P.P. Aurino, R. Gunnarsson, D. Winkler, E. Olsson, N. Tuzla, J. Börjesson, Y. Cao, L. Nyborg, Y. A. Boikov, I. T. Serenkov, V. I. Sakharov and M. P. Volkov, *"Inhomogeneous Microstructure and Electrical Transport Properties at the $LaAlO_3$/SrTiO3 Interface ",* JJAP **51,** 11PG10 (2012).

D. A. Kalabukhov, T. Claeson, P.P. Aurino, R. Gunnarsson, D. Winkler, E. Olsson, N. Tuzla, J. Börjesson, Y.A. Boikov, I.T. Serenkov, V.I. Sakharov and M.P. Volkov, *"Electrical and structural properties of $ABO_3/SrTiO_3$ interfaces",* MRS Proceedings, 1454, pp 167-172, doi:10.1557/opl.2012.925. (2012)

Table of contents:

1. Introduction 1

1.1 Background 2

1.2 Aim of this work 4

2. Thin film growth 5

2.1 Thin film growth 5
2.1.1 General concept 5
2.1.2 Lattice mismatch 6
2.1.3 Film growth modes 7
2.1.4 Thermodynamic conditions 8

3. Materials 9

3.1 Oxide interfaces with high electron conductivity and mobility 9
3.1.1 Transition metal oxides 9
3.1.1.1 $SrTiO_3$
3.1.1.2 $LaAlO_3$ 11
3.1.2 $LaAlO_3/SrTiO_3$ 12
3.1.2.1 Thickness dependence 12
3.1.2.2 Oxygen pressure during growth dependence 12
3.1.2.3 Depth of the conducting region 14

3.2 Fluorite type oxide electrolyte with high ionic conductivity and mobility 14

3.2.1 Fluorite type oxides 14
3.2.2 Yttrium Stabilized ZrO_2 15

3.2.2.1 Ionic conductivity in bulk YSZ 17
3.2.3 Nanostructured YSZ 18
3.2.3.1 Increase of ionic/electronic conductivity in nanostructured YSZ 18
3.2.4 Microstructure of YSZ thin films 19
3.2.4.1 Crystal orientation 19
3.2.4.2 Oxygen pressure and thermal effect 20

4. Interfacial phenomena 21

4.1 Two dimensional electron gas at oxide interfaces 21
4.1.1 Background to 2DEG 21
4.1.2 Polar discontinuity at interfaces 22
4.1.2.1 Polar catastrophe 23
4.1.3 Oxygen vacancies 24
4.1.4 Doping by cation interdiffusion 24

4.2 Ionic conductivity of nanostructured materials 25
4.2.1 Introduction to microstructure aspects 25
4.2.2 Grain boundary contribution 26
4.2.3 Charge carrier mobility along the interface between nanostructured film and substrate 27

5. Experimental methods 29

5.1 Investigated samples 29
5.1.1 LAO/STO 29
5.1.2 YSZ/STO & YSZ/LAO 29

5.2 Sample fabrication 30
5.2.1 PLD 31
5.2.2 RHEED 32

5.3 Electrical characterization 33

5.4 Structural characterization methods 35
5.4.1 AFM 35
5.4.2 X-Ray Diffraction 36

5.4.3 Electron Microscopy 38
5.4.3.1 TEM setup 39
5.4.3.2 Imaging 42
5.4.3.3 HRTEM 44
5.4.3.4 Electron diffraction 45
5.4.3.5 STEM 46
5.4.3.6 HAADF STEM 48
5.4.3.7 EDS 51
5.4.3.8 Sample preparation 52

6. Summary of appended papers 55

6.1 PAPER I 55
6.2 PAPER II 55
6.3 PAPER III 56
6.4 PAPER IV 56
6.5 PAPER V 57

Acknowledgement 59

Bibliography 61

1

Introduction

The plethora of useful physical properties has made complex oxides a subject to intense research during the last decades. The properties are determined by the details of the structures at very small length scales. The ability to grow oxide thin films with atomic-layer precision opens the possibility to tailor the properties and for them to play an important role in future electronic devices. Often the interfaces between thin films in multilayers and also at the interface between a film and the substrate introduce new properties. The interfaces generate an astonishing range of novel physical phenomena resulting from the interplay between charge, spin and strain. A combination of different oxides, can offer interfaces and/or super lattices with new and improved physical properties.

1.1 Background

The tremendous interest in oxides arises from the fact that no other class of materials exhibits such a diverse range of properties. Some of the novel properties which can be found in different combinations in complex oxides are a whole range of the electronic properties from insulating to superconducting [1], including the wide range of bandgaps, low-k and high-k dielectric properties ranging all the way to ferroelectric [2] and piezoelectric as well as a difference in the surface chemical reactivity.

The efficiency of these oxides is directly linked to the quality of the oxide material used. Hence, future technologies require fabrication of these materials with a high degree of control. To reach this task we need to understand the factors that control the properties of the oxides, both from a scientific and a technological viewpoint.

The thin film properties of complex oxides usually differ from the bulk material. A more obvious and fundamental parameter is reduction of one dimension of the crystal to sometimes only a few unit cells. This results in the possibility of almost 2-dimensional structures with different behavior with important implications for the fast developing nanotechnology. The ratio of interface atoms to bulk atoms become very high in these structures, which promotes the dominating influence of interfaces on the nanostructured materials. Hence, the properties of these materials can differ drastically from the bulk properties.

The structure-property relation of thin film oxide interfaces is determined by parameters like film thickness, interfacial boundary, grain size, crystal orientation, etc., which are in turn effected by the growth method and growth parameters.

The fabrication of these materials has progressed tremendously in the last 15 years. Well controlled thin film growth on the atomic scale and a possibility to choose single-terminated substrate surfaces, enabling well defined interfaces, is now a possibility with pulsed laser deposition (PLD) and in-situ reflective high energy electron diffraction (RHEED).

Also the analysis techniques like high-resolution scanning transmission electron microscopy, become more advanced and are able to more reliably and in detail provide information about the structure and composition of these complex oxides. All these recent advances within fabrication and analysis techniques are helping the scientists today to bring forward new questions that crucial for further understanding of thin film heterostructures.

In this thesis work the focus is on studying two different interfacial phenomena. One is the interface between two perovskites, two insulating complex oxides with very similar u.c. parameters; $LaAlO_3$ (LAO) and $SrTiO_3$ (STO). These two insulators,

when combined with each other specifically so that LAO is epitaxially grown on TiO_2-terminated $SrTiO_3$ (001), exhibit what appears to be a two-dimensional electron gas (2DEG) at the interface. This interface shows a full range of useful properties and raises a lot of interesting questions. Meanwhile, depending on the growth parameters, the properties of the interface vary. The very same interface can appear as insulating, semiconducting or low-temperature superconducting and ferromagnetic. At very low $p_{O2} < 10^{-5}$ mbar oxygen vacancies (Vo) are formed as a result of deficient oxidation, causing conductivity. Moreover, the perception of the underlying mechanism for this conductivity has lately grown stronger in two separate paths. One is that atomic structure reconstruction and/or intermixing occurs close to interface in samples grown at p_{O2} 10^{-3}-10^{-4} mbar, and the other is a polar catastrophy model.

LAO and STO belong to a class of complex oxides called transition metal oxides that contains a wide variety of physical properties, due to the electron correlation nature of these materials. These are particularly interesting due to the strong directionality of the outer electron orbitals in the material. The high directionality is causing a high probability for electron-electron interaction. The consequence is that small changes in crystal structure will manifest itself in a change of physical properties. Another important issue is that the change of number of electrons in the core shell of many of the transition metal oxides does not result in a changed ion core state. Instead these adapted electrons contribute to the electron correlation from the outer shell. These aspects show that complex oxides are perfect building blocks for studying electronic correlations at the nano-scale.

Furthermore, integrating nanostructured oxides with large lattice mismatch parameters, into relatively ordered crystalline structures, has lately gained increased interest, with the hope for enhanced functional properties. Thus, a second type of interface that will be discussed in this work, is the interface between the unique structure of the fluorite type oxide – Yttrium-stabilized Zirconium (YSZ) and perovskite type oxides, ABO_3. Bulk YSZ is a good ionic conductor at elevated temperatures, and is widely used as electrolyte material in oxygen fuel cells. Furthermore, there is a larger mismatch coefficient between its unit cell parameter and a typical perovskites. These interfaces have caused the electrical conductivity to increase by up to an order of 8 times. Nevertheless, the mechanism causing the increase of electronic/ionic conductivity is still not fully understood neither is the dominating driving force for the specific arrangements of the film structure.

Understanding the properties of these tiny devices and being able to tailor them according to desire is one of the most challenging tasks of the last decades.

1.2 Aim with this work

The objective of my thesis work is to gain a fundamental understanding of how the microstructure at oxide interfaces influence the properties. The studies are carried out by correlating the structure of the interfaces on the nanoscale level to its influence on the electrical transport.

One part of this work is concentrated on understanding the origin of the electrical conductivity at the interface between the two insulators; $LaAlO_3$ and $SrTiO_3$. Another part is focusing on how interfacial structure modifications between stabilized zirconia thin films and ABO_3 perovskite type oxides may lead to an enhanced conductivity performance.

The thin film and interface structures are studied using analysis technique enabling sub-ångström resolution -transmission electron microscopy. Methods like Z-contrast imaging, electron diffraction and energy dispersive X-ray (EDX) analysis are used, along with X-ray diffraction (XRD), atomic force microscopy (AFM) and Rutherford high energy electron diffraction (RHEED) combined with data on the prop.

2

Thin film growth

2.1 Thin film growth

2.1.1 General concept

Thin films of complex oxides are achieved by growth on top of another material surface. The growth process depends on the transportation mechanism of material to the substrate surface. Depending on the growth method, the adsorbed material can be in different states, liquid, vapor or solid. In this work, the *Pulsed Laser Deposition* (PLD) technique have been used for the growth of thin films. The basics of how this technique is working are explained in Chp.5. In PLD solid matter nucleates on the substrate surface from an unstable vapor phase. Hereby a vapor-solid interface is established with a corresponding interfacial energy, before the condensation reaction occurs along with the reduction of the surface free energy.

Interfacial energy, or surface energy, is the access energy a surface atom contains in comparison to an atom within the underlying bulk. It is originating from the fact that surface atoms make fewer bonds with the surrounding and are thereby less constrained and posses more energy. There is a thermodynamic desire to reduce the number of free bonds if possible, by re-bonding between atoms. *Heterogeneous* nucleation, nucleation between the re-condensed film on the substrate, is dependent on interplay between several variables; substrate temperature, deposition rate and critical film nucleus size. When the incoming material first comes in contact with the surface, it is through weak bonding. In this way the material species is allowed to migrate or *diffuse* along the sample surface until it finds an energetically favorable position and strongly binds (= *chemisorbs*) to the surface lattice. Step ledge, kink,

vacancy in the terrace or nucleus at the terrace are all examples of such positions. The average distance of material surface diffusion is sensitive to the parameters like substrate temperature and the energy of the incoming material. In conclusion, film growth is a complex phenomenon, where the outcome depends on all the above-mentioned parameters. The most important film growth modes are described below.

2.1.2 Lattice mismatch

An important issue to address separately is the lattice mismatch between the film and the substrate they are grown at. The lattice mismatch can cause strain effects, which can have conclusive effects on the properties of the film, interface and a combination of those [3]. It can cause dislocations in the film, surface roughness can be changed and it can change ionic disorder, or cause change of the transition temperature. If the thickness of the film is above a certain critical thickness, the strain caused by lattice mismatch is compensated by defects in the film, whereby it reduces its internal energy. Misfit dislocations or changes in composition, can allow the film to rearrange to more bulk-like dimensions. However, if the film is kept thin, i.e. below the critical thickness, its lattice will be strained to fit with the substrate, either by compressive or tensile strain.
Lattice mismatch is defined as the difference between the size of the two lattice units of film and substrate ($a_s - a_f$, direction along the interface), divided by the length of the lattice unit of the substrate, a_s. This will then give lattice mismatch values of 2,9%, 4,1% and 7,1% for (001)LAO/(001)STO, (001)YSZ/(001)LAO and (001)YSZ/(001)STO respectively.

For epitaxial growth, preferably complex oxides with matching lattice parameter are suitable substrate materials. In such cases strain can cause distortion of the oxygen octahedral in complex oxide lattice and it may manifest it self in change of the electronic system behavior. Electronic properties of oxides are determined by the nature of the cation-oxygen bonding. The bonding is a result of a balance between the kinetic energy and Coulomb repulsion. Hereby, upon slight change of the strain, different phases with energetically different ground states are obtained. Consequently, the interface performance is also influenced by the terminating atomic layer of complex oxide thin films.
Subsequently, all these factors have conclusive effects on the properties of the film, interface and a combination of those. They can cause dislocations in the film, surface roughness can be changed as well as ionic disorder.

2.1.3 *Film growth modes*

Layer-by-layer growth (Frank der Merwe growth):

In this growth mode intermediate temperatures are used to ensure the appropriate surface diffusion length of the adsorbed species, i.e. shorter than the average terrace width, but large enough for the islands to continue to grow in-plane until the first layer totally covers the step of the substrate surface step. This will then provide for island nucleation on the terraces, but first after the previous layer have been completed. This process is then repeated for each monolayer and is called coalescence. This growth mode prefers low lattice mismatch. Conditions for layer-by-layer growth are that the adsorbed species, while still in vapor state, are more strongly bonded to the underlying layer than to the nearest neighbor in the film.

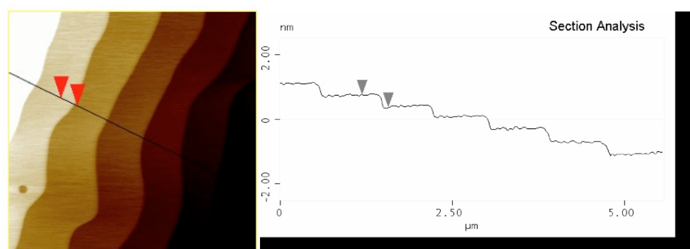

Figure 1: To the left: AFM image of the LAO/STO sample surface after the film deposition using the PLD. To the right: Side view of the sample surface showing flat terraces separated by steps corresponding to 1 uc hight of LAO and approximately 700 nm wide.

Island growth (Volmer Veber growth)

In some cases, surface tension of the growing film material can be higher than that of the substrate. Due to a driving force to minimize the surface tension area, the material will tend to cluster around a nucleation site, which in turn gives rise to an island growth. This mode is common for materials with large lattice mismatch, which will cause a preference of the incoming material to diffuse to the material with same structure, at which it will chemisorb. The result will be growing islands in three dimensions.

Layer plus island growth (Stranski-Krastanow growth)

Typical for this growth mode is that the film starts to grow as a layer-by-layer until a certain thickness, when it suddenly changes to island growth. This growth mode has been observed for similar materials with large mismatch. Most probably, the

relaxation of the accumulated strain energy is due to the increasing strain energy with increasing film thickness. At the moment of transition of the growth mode, the energy of the strained film surface has reached a critical level and the film relaxes, by forming misfit dislocations. These dislocations change the conditions causing the island growth.

2.1.4 Thermodynamic conditions

As mentioned earlier, the parameters used during the deposition of the film have crucial influence on the microstructure and thereby also on the conduction properties. The oxygen deposition pressure is a crucial parameter for achieving stable phases of the oxide and can be used to achieve desired properties of the film, as will be discussed further on in this thesis. Furthermore, high growth temperatures, i.e. substrate temperatures are usually applied during epitaxial growth of complex oxides, because that promotes the growth kinetics. Higher substrate temperature has several important effects, like increasing the size of the critical nucleus, increasing the typical size islands and decreasing the number of the so-called critical nuclei, whereby increased time is needed to grow a continuous film.

The crystallographic orientation of the film is determined by the interactions at the initial stage of the in situ growth. However, sample-treatment after the deposition, i.e. during cool-down to room temperature, also affects the microstructure. The difference between the thermal expansion coefficients of the film and the substrate material can induce extra strain during the cool-down process.

The microstructure is very sensitive to the environmental conditions and even minor differences during heating and cooling may cause significant changes. Large crystallites or epitaxial films are preferably obtained using high substrate temperatures at low deposition rates.

In summary, the most common case is that several of the above-mentioned effects are in action during film growth. Understanding the properties of the nanoscale devices and being able to tailor them according to desire is one of the most challenging tasks during the last and coming decades. Oxide thin films exhibit a wide variety of important properties, like high resistivity against corrosion, structural compatibility with each other and other already mentioned novel properties. The objective is to fabricate and study complex oxides with a high degree of control of the composition and morphology.

3

Materials

3.1 Oxide interfaces with high electronic conductivity and mobility

3.1.1 Transition metal oxides

Transition metal oxides are a class of complex oxides with a wide variety of physical properties, due to that the electrons in these compounds are strongly correlated and and there is also an orbital degree of freedom. This means that the outer d-electrons of the ions in the systems can choose between different orbitals, which in turn strongly influences the properties., The electrons interact with each other also adding to the variety of properties. The consequence is that small changes in crystal structure will manifest themselves in changes of physical properties. The combination of different oxides offers unique symmetries at the interfaces, which can result in a variety of useful effects, like magnetism, superconductivity, metal-insulator transition, multiferroicity, where LAO/STO thin film systems is one example. Another important issue is that the change of number of electrons in the core shell of many of the transition metal oxides does not result in a changed ion core state. Instead these adapted electrons contribute to the electron correlation of the outer shell.

Perovskites are a structural family that belongs to transition metal oxides, having the general structural formula ABO_3, see Fig 2. 'A' and 'B' are two sites containing different elements, with the oxygen atoms surrounding the B site at the face center positions. ‘A’ site consists of either a metal element from group one or two in the periodic table or a lanthanide. ‘B’ site consists of a metal that has a d-electron as a valence electron.

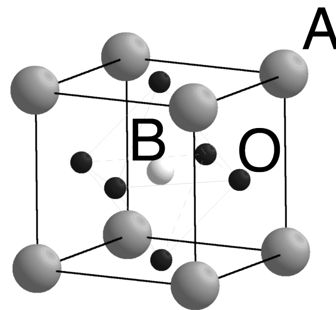

Figure 2: Schematic of the ABO_3 perovskite unit cell. This particular figure corresponds to the ideal cubic perovskite unit cell, with the crystallographic formula $Pm\bar{3}m$.

Perovskites can have cubic, tetragonal, orthorhombic, rhombohedral and even monoclinic crystal structure [4]. They also show a wide range of different properties, like metallic, semiconducting, insulating and superconducting. Moreover, a phase transformation can be caused by a change of temperature through a critical temperature and thereby change the properties. Compositional variations like oxygen content, electronic configuration and nature of atomic bonds, often dramatically change the physical properties in these systems. $SrTiO_3$ is a good example of those property-variations as described in the next section.

Some combination of metals at A and B sites can cause tilting or elongation of the oxygen octahedral, which play a central role in properties of many oxide compounds. This results in a slight distortion of the ideal perovskite cell. A tetragonal structure is obtained when some of the B-site metals split the degenerate orbital levels and cause a so-called Jan-Teller distortion (elongation) of the BO_6-octahedra [5]. Several different distorted structures from the ideal perovskite, like tetragonal, orthorhombic and hexagonal, can be obtained by tilting the oxygen octahedra.

3.1.1.1 $SrTiO_3$

$SrTiO_3$ has become a very attractive material for research in the microelectronic industry of several reasons. It shows many valuable functionalities, like being a high-K dielectric material [6], wide-band gap material (3,2 eV) [7,8] and covering wide range of electric conductivity upon doping with oxygen vacancies.

$SrTiO_3$ belongs to the group of transition metal oxides and has a cubic perovskite structure above 106K with the space group $Pm\bar{3}m$ [9]. Bulk $SrTiO_3$ at room temperature has a lattice parameter 3,905Å [10], which makes it a good match to many other perovskites and thus makes it very suitable as a substrate material for epitaxial growth of thin films.
The Sr atoms are positioned at A-sites and Ti atoms at B-sites in the perovskite unit cell, leading to a stack of alternating $Sr^{2+}O^{2-}$ and $Ti^{4+}O^{2-}{}_2$ layers. These ionic distributions are the possible terminations of the (001) crystal surface.
Today it is possible to obtain single terminated surfaces [9,11], but the complete understanding of the atomic surface structure and the forces that control it is not yet reached.

$SrTiO_3$ electrical properties can be altered upon doping with La, Ta and Nb, changing the insulator into an n-type conductor or even a superconductor in some cases at very low temperatures [12,13]. Furthermore, introducing small amounts of oxygen vacancies also dopes the $SrTiO_3$ [13,14,15], with free states in the band gap and thus adds electrons in the conduction band. $SrTiO_3$ bulk crystal is usually colorless, but can change color upon doping.
Dependending on annealing conditions different reconstructions of the $SrTiO_3$ occur during thermal treatment. Annealing at high temperatures (800 – 1400°C), beyond the re-crystallization temperature before cooling causes an oxygen deficiency [16]. An oxygen deficiency is also reached by deposition of an oxygen-reduced film [16], or by treatment with Ar-ions.

3.1.1.2 $LaAlO_3$

$LaAlO_3$ has rhombohedral perovskite structure at room temperature, which is slightly distorted from the cubic perovskite. It has a band gap of 5,6 eV and is thus a wide band gap insulator. The lattice parameter is 3,79 Å and it belongs to the spacegroup $R\bar{3}c$. The alternating ionic layers that build up the material are $La^{3+}O^{2-}$ and $Al^{3+}O^{2-}{}_2$.

3.1.2 $LaAlO_3$/$SrTiO_3$

A highly conducting layer forms at the interface between thin films of $LaAlO_3$ and $SrTiO_3$, wide band gap insulators, under certain circumstances. This was first reported by Ohtomo et.al in 2004 [17] and soon it became the most explored interface with a conducting electron gas. An important reason or this enormous interest is the wealth of intriguing properties that this material possess, as well as the ease with which these films can be grown. There are three main proposed mechanisms explaining the observed two-dimensional electron gas at the LaO/TiO_2 interface of $SrTiO_3$/$LaAlO_3$ heterostructure: Polar catastrophe [18], oxygen vacancies [19,20,21,22] and cation intermixing [23,24], which will be addressed in next chapter.

3.1.2.1 Thickness dependence

Soon after the discovery of the conductivity, it was clear that the thickness of the $LaAlO_3$ thin film strongly affects the performance.
Measurements of the sheet conductivities and carrier densities at the n-type interface show that the interface conductivity changes very abruptly as a function of the number of $LaAlO_3$ unit cells. According to experiments, the critical thickness occurs at 3 – 4 unit cells [25] and can be reduced under an applied electric field [26]. A common conclusion resulting from the critical thickness observation is that for certain thickness of $LaAlO_3$ films, the electrostatic potential difference, caused by the polar discontinuity at the interface, must be relaxed. The relaxation takes place through a reconstruction at the interface that can be either electronic or ionic. Electronic reconstruction involves a transfer of electrons from $LaAlO_3$ to most likely Ti 3d conduction band in $SrTiO_3$. The ionic reconstruction refers to lattice distortions and cationic intermixing. Both reconstructions could thus explain the conductivity that raise up at the interface.

3.1.2.2 Oxygen pressure during growth dependence

Another important observation of factors that influence the conductivity at $LaAlO_3$/$SrTiO_3$ interface was the effect of applied oxygen pressure during the growth of the film. It became clear that higher oxygen pressure reduced the conductivity and could even result in an insulating behavior [19,27], and that films grown at low oxygen pressure (10^{-6} mbar) instead were highly conductive.
In Fig. 3 a diagram showing the relation between conductivity and oxygen growth pressure is presented.

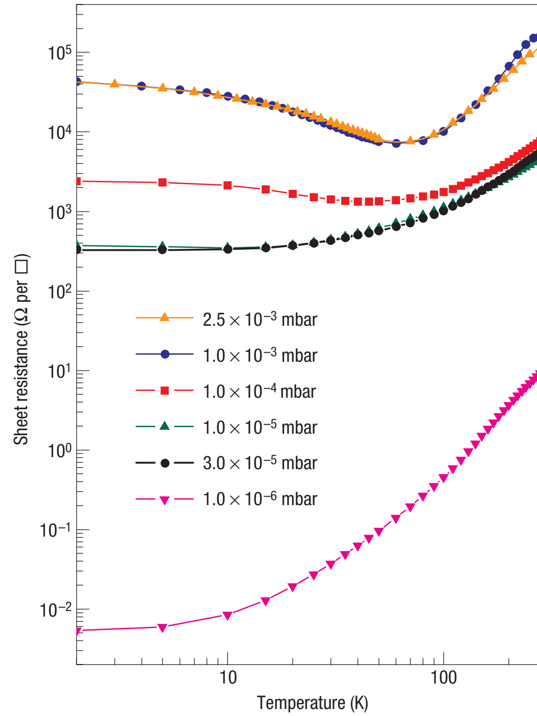

Figure 3: Sheet resistance as a function of temperature for thin films grown at different oxygen pressures [19].

It has already been mentioned that oxygen vacancies, which are created during the growth of the $LaAlO_3$ film, can dope the $SrTiO_3$ with electrons and thus provide free charge carriers. Studies on $LaAlO_3/SrTiO_3$ interfaces show evidence of polarity-induced oxygen vacancies at interfaces grown at low oxygen pressures (10^{-6} mbar) [18,28]. In [28] the authors also point out the fact that it is still not possible to exclude the formation of oxygen vacancies, induced by polarity of $LaAlO_3$ even for conducting samples grown or annealed at higher oxygen pressure than 10^{-6} mbar, which is consistent with their theoretical calculations. However, as already mentioned, the oxygen vacancies are not the only source for the conductivity in films grown at higher oxygen pressures (10^{-4} mbar). At this oxygen pressure range it is commonly believed by now that the "Electronic rearrangement at the surfaces " or the ionic mixing is doping the $SrTiO_3$ surface, making it conductive as well.

Kalabukhov *et al* experimentally investigated $SrTiO_3$ substrate as well as $LaAlO_3/SrTiO_3$ heterointerfaces, deposited at different oxygen pressure conditions, by comparing photoluminescence and cathodoluminescence in combination with HRTEM results [20]. Typical growth conditions were used when growing the $LaAlO_3$ films on $SrTiO_3$ substrates. The same conditions were applied for the growth of $SrTiO_3$ alone. Moreover, $SrTiO_3$ was subject to Ar-ion bombardment, which induced oxygen vacancies. In conclusion, all three sample types always showed increased resistivity upon oxygen annealing. Moreover, the authors also pointed out that it is not

possible to exclude that oxygen vacancies in $SrTiO_3$ prepared at high oxygen pressure are the only reason for the conductivity.

3.1.2.3 Depth of the conducting region

In search for an explanation for the nature of the conductivity at the $LaAlO_3/SrTiO_3$ interfaces, there have been several publications on the depth of the conducting region. Kalabukhov et al noticed very high charge-carrier densities at these interfaces, much higher than the expected values for such a polar interface [20]. These results were therefore interpreted in terms of a conducting region that includes the bulk of the $SrTiO_3$ instead of only the interfacial region.
Several other investigations supported these results, like the one by Herranz et.al. [29] where Shubnikov-de Haas oscillations were used to measure the depth of the conducting layer into the substrate, which was found to be over hundreds of microns for low oxygen pressure samples. A more extended investigation was performed on this topic, where cross-sectional samples (films grown at $5x10^{-5}$ mbar) were subject for investigation with a conducting tip AFM measurements [30]. These studies showed that there was distinct difference between non-annealed and post-annealed samples, where first kind showed a slowly decreasing resistance from the substrate into the interface, while the latter case showed an abrupt decrease of the resistivity approximately 7 nm from the interface. Lately different probe techniques revealed that the conductivity in samples grown in lower oxygen pressure regime was indeed confined to the 1 – 10 nm region at the interface [30,31,32,33], and even to only a few uc from the interface. They however also found that it was a temperature dependent effect.

3.2 Fluorite type oxide electrolyte with high ionic conductivity and mobility

3.2.1 Fluorite type oxides

Fluorite type oxides are oxides arranged in fluorite type crystal structure, with general formula AO_2, represented in the Fig. 4. A is usually a big tetravalent cation, like U, Th, Ce or Zr^4, arranged in a face-centred-cubic structure with the oxygen anions in the tetrahedral sites. Arranged in this way, the anions have a coordination number of 4, while the cations have 8*.

Some of these material compounds have a tendency to have vacancies on the anion lattice sites, which makes them good ionic conductors. One such compound is $Y_XZr_{1-X}O_{2-X/2}$ or Yttrium stabilized Zirconia.

* Coordination number of an atom is the number of other atoms that it touches, in a model where atoms in a crystal are represented by touching spheres.

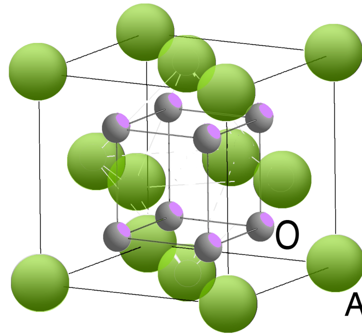

Figure 4: Simple model of a cubic fluorite type $Fm\overline{3}m$ *unit cell.*

3.2.2 Yttrium stabilized ZrO_2

Pure zirconia (ZrO_2) is polymorphic, stabilizing into three different stable crystal structures depending on the temperature [34]. This makes it an interesting candidate for different applications. However, stabilizing zirconia with a larger dopant, i.e. replacing the small Zr^{4+} cation with a larger one with lower valence (X^{3+} or X^{2+}), makes it sustain (or almost sustain) the cubic fluorite structure throughout the temperature range. Fig. 5 illustrates the doping process, where Y_2O_3 is used as a dopant.

.

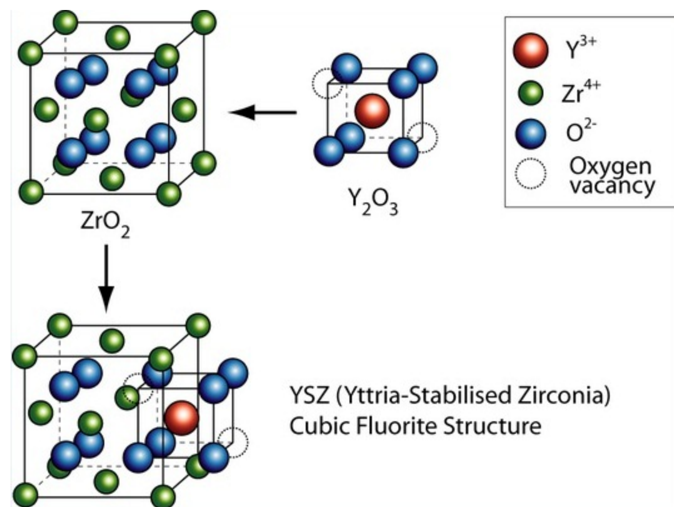

Figure 5: Simple model of the doping process where Y_2O_3 dopes the ZrO_2

Cubic fluorite type yttrium stabilized zirconia belongs to the spacegroup $Fm\overline{3}m$ and has a lattice parameter of 5,14Å. Another big advantage gained from the Y stabilization process is the high ionic conductivity, obtained from resulting the oxygen vacancies by maintaining charge neutrality (see next chapter). However, at low temperatures, low vacancy mobility limits the oxygen ion mobility.
More on the mechanisms giving rise to the ionic conductivity will be discussed in next chapter.

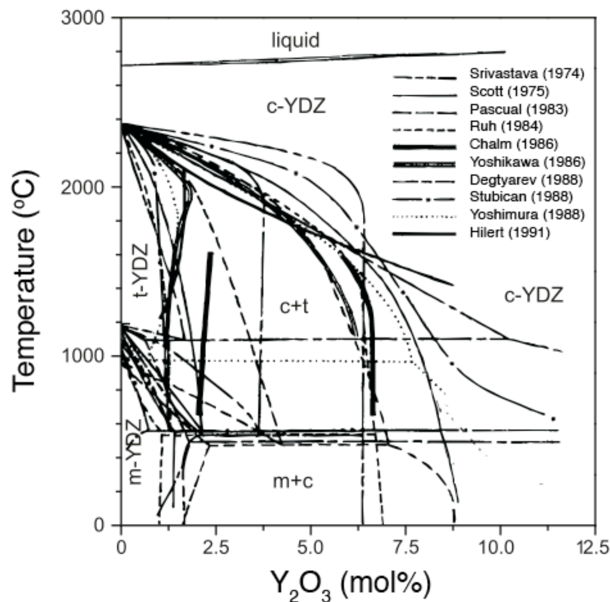

Figure 6: Phase diagram of YSZ, redrawn after [35].

Besides the stable cubic fluorite phase at different temperatures, YSZ show many good characteristics that makes it a valuable material in many different areas. Due to its high ionic conductivity, YSZ is well suited to be used as electrode material in solid oxide fuel cells (SOFC), at temperatures ≥ 800°C. YSZ is not the best ion conductor, but it is the cheapest to process and has low enough electronic conductivity. There are many other materials that are better ionic conductors but a combination of different advantages of YSZ makes it the most suitable electrode material at present. Other useful properties are: high chemical stability and hardness even at elevated temperatures, it is a good thermal insulator and it is non-toxic. Examples of other areas where YSZ is found to be useful is the material for tooth crowns, thermal barrier coating material in gas turbines and oxygen sensors.

3.2.2.1 Ionic conductivity in bulk YSZ

Pure zirconia shows very low ionic conductivity, which can be explained by very low concentration of intrinsic defects. However, as already mentioned, the oxygen vacancies are introduced into the ZrO_2 structure through doping with cations with larger ionic radius and lower oxidation state. Introducing one Y_2O_3 molecule into the ZrO_2 structure produce a single additional oxygen vacancy according to following equation:

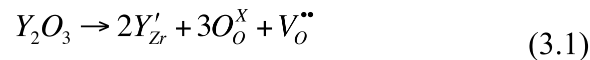

$$Y_2O_3 \rightarrow 2Y'_{Zr} + 3O_O^X + V_O^{\bullet\bullet} \quad (3.1)$$

Here the Y'_{Zr} represents the Y ions that have replaced the Zr on the cationic sites, reducing the charge with -1. O_O is the regular oxygen ion on the anionic site. $V_O^{\bullet\bullet}$ is the oxygen vacancy that is +2 charged in respect to the charge of regular oxygen ions. This logically leads us to understanding that by knowing the concentration of Y ions, it directly leads us to the concentration of vacancies. Having this in mind it would be easy to assume that the conductivity is directly proportional to the number of vacancies in the material, but this is wrong. Extensive studies have been performed on YSZ investigating exactly this, as a function of temperature [36,37,38]. They all agree about the result, showing that the highest conductivity is obtained upon doping the ZrO_2 with 8–9 mol% Y_2O_3, no matter what temperature is used. Using higher concentrations of dopants only cause the conductivity to decrease. Besides depending on the oxygen vacancy concentration, the ionic conductivity also depends on the mobility of the vacancies. The net ionic current depends on applied electric field. The ionic conductivity is usually described by the Arrhenius equation,

$$\sigma = \frac{A}{kT} exp\left(\frac{-E_a}{kT}\right), \quad \text{where} \quad A = \frac{1}{3}(Ze)^2 n d^2 \omega_0. \quad (3.2)$$

Here σ is the ionic conductivity, k is the Boltzmann constant, T the temperature, E_a is the activation energy for ion migration, Ze is the charge of the migrating ion, n is the vacancy concentration, d is the ionic diffusion distance unit and ω_0 is the frequency. The mobility, μ, is connected to the conductivity according to the following equation:

$$\mu = \frac{e\sigma}{n(Ze)^2} \tag{3.3}$$

The mobility depends on the interaction between different factors, like the randomness of defect concentration, the ionic radius of the dopants (relation in ionic size between Y^{3+} and Zr^{4+}) and the microstructure of the material. The oxygen vacancies diffuse through the anionic sublattice in the bulk as well as across and/or along the internal defects like grain boundaries and cracks if such exist. Defects change the symmetry and cause a sudden change of vacancy concentration.

3.2.3 Nanostructured YSZ

The disadvantage of the high working temperature of YSZ electrolytes has lately spurred an interest in decreasing it to about 400 – 600C. However, the ionic conductivity of bulk YSZ in this temperature range is still too low for practical applications in fuel cells. Now there is a hope that the ionic conductivity can increse at interfaces between thin epitaxial films of YSZ and other materials, due to the nano-sized effects. In these small dimensions the surface, interface and grain boundary effects become very pronounced, compared to the bulk materials. Hence, they can in some cases dominate over the properties of the whole material, changing them drastically.

The combination of fluorite/perovskite heterostructures has attracted interest since recent studies on such nanoscaled systems have shown conductivity increase related to the grain boundary and interfacial effects. However, we still lack the fundamental understanding of the origin of this increase between large misfit structures. These nanostructured systems have already showed potential to be used in solid oxide fuel cells applications as well as gas sensors and ionic membranes.

3.2.3.1 Increase of ionic/electronic conductivity in nanostructured YSZ

In 2005 Kosacki et al. [39] reported that the ionic conductivity in epitaxial YSZ (100) thin films on MgO (100) is increased up to 2 orders of magnitude when the film thicknesses is reduced below 60nm. This was attributed to an increased level of disorder at the interfacial region. An increase of ionic conductivity by up to one order of magnitude in YSZ/Y_2O_3 superlattice fabricated on sapphire when the thickness of YSZ films decreased from 526 nm to 24 nm, was reported by Korte et al. [40]. This

was explained by strain effects in the YSZ thin films. Sillassen et al. [41] fabricated YSZ epitaxial thin films on $StTiO_3$ and MgO single crystal substrates by RF magnetron sputtering. They reported an up to 3 order of magnitude enhancement in ionic conduction of these epitaxial YSZ thin films. The enhancement of the ionic conduction was proposed to be caused by strain of YSZ film due to lattice mismatch with $SrTiO_3$ and MgO substrates. J. Garcia-Barriocanal et al. [42] reported up to 8 orders of magnitude increase in the ionic conductivity in YSZ/$SrTiO_3$ heterostructures. This is the highest reported ionic conductivity related to YSZ. Cavallaro et al. [43] reported fabrication of the polycrystalline YSZ/$SrTiO_3$ heterostructures by PLD under conditions similar to used in [42] and attributed the observed enhancement to the electronic rather than ionic conductivity.
Pennycook et al [44] found evidence of disordered YSZ O sublattice at both the coherent interfaces of YSZ/$SrTiO_3$ multilayers as well as at incoherent interfaces between YSZ islands with surrounding $SrTiO_3$. It is recognized by blurred out fine structure in this region comparing to the surroundings, supported by both theoretical simulations as well as experimental results. These results support a strain induced oxygen sublattice disorder and indicate this to be the origin of colossal ionic conductivity.

The diversity of the results obtained from different investigations of thin films and superlattices of YSZ, show the big potential in possible enhancement of the desired properties. However, they also show the huge lack of basic understanding of ionic conductivity mechanisms. Better understanding of what is going on in these structures requires detailed investigation of the microstructure on the atomic level.

3.2.4 Microstructure of YSZ thin films

In this section already reported results found for YSZ nanostructures are presented. Further discussion about the proposed mechanisms for the conductivity in YSZ thin films can be found in next chapter

3.2.4.1 Crystal orientation

A nano crystalline microstructure is believed to be able to increase the transport properties. In order to understand the fundamentals of the conductivity mechanism in these materials one crucial step is to figure out the connection between the growing parameters and the microstructure.

Cavallaro et al [45] investigated PLD grown multilayers of YSZ/$SrTiO_3$, at 900°C and 4,7 Pa oxygen pressure during growth. They show 15°-tilted (111) YSZ oriented domains as well as the 45° in-plane rotated (001)YSZ//(001)$SrTiO_3$ domains. Later it was reported that YSZ films grow with different orientation dependent on the

substrate termination and that SrO terminated $SrTiO_3$ substrate surface favors 45°-in plane rotation of 100 YSZ, while TiO_2-termination induces island growth containing of 10°-15° tilted (111)-YSZ domains [45]. Several other publications show evidence of the 45°-in plane rotated (001)YSZ//(001)$SrTiO_3$ orientation for films grown at both higher and lower oxygen pressures, without mentioning traces of the (111) orientation [41,42,44].
There are reports in the literature where YSZ was grown on other substrates like silicon [46], Pt/SiO_2 [47] and sapphire [48] at similar deposition circumstances. In these cases YSZ films were found to be preferentially (111) orientated with some fractions of (100).

3.2.4.2 Oxygen pressure and thermal effect

In addition to the lattice orientation of the grains, the last two papers also report on the possibility to control the grain size and surface roughness by varying the growing conditions by choosing different oxygen pressure. Increasing oxygen pressure causes the films to be more rough with larger grains [48] and more porous [47]. This information can be very important, since the porosity can affect the conducting area along the film and thereby reduce the overall conductivity.
Shin et.al. [49] have also reported on the impact of oxygen partial pressure during the pulsed laser deposition on the morphology of YSZ films on glass. However, measurements of the roughness were performed in a rather high oxygen pressure range, 10^{-2} – $1,3*10^{-1}$ mbar, which resulted in a roughness 3 - 30 nm, for films with thickness of 600 – 1000 nm.

The oxygen pressure impact on the surface roughness of polycrystalline films has been explained previously. According to this theory, high oxygen pressure is supposed to accommodate large ionic clusters, which are formed in the plasma plume during the PLD ablation process [47,50]. Due to a reduction of mean free path of gas particles at high oxygen pressure, oxygen molecules and in this case zirconium ions can easier meet and thereupon form reactants. If these clusters posses higher binding energy than the energy at the substrates (i.e. kinetic plus thermal), they maintain their shape and form porous films on the substrate surface. As the thermal energy of the substrate increase, by increased substrate temperature during deposition, larger columnar grains can be formed.

4

Interfacial phenomena

4.1 Two-dimensional electron gas at oxide interfaces

4.1.1 Background to 2DEG

The definition of a two dimensional electron gas (2DEG) is that it is a gas of electrons, which are free to move in only two dimensions. In bulk materials of metals and semiconductors, the charge carriers are free to move in three dimensions. The two dimensional confinement can be achieved in different ways, such that the resistance perpendicular to the conducting plane is very high. Well-known examples of such 2D systems are a single graphite sheet layer and a semiconductor-oxide interface in silicon MOSFET transistor. The latter one was the first system in which the physics of 2DEGs was studied. It is based on the one dimensional model of the particle in the box. Depending on the externally applied potential, electrons are confined to specific energy levels. This model can be extended to a two-dimensional case, where the potential well in the third dimension allows the electrons to move freely in the plane perpendicular to it.

About a decade ago, 2DEG was found at the heterointerface (interface between polar and non-polar materials) between two wide band-gap transition metal oxides, $LaAlO_3$ and $SrTiO_3$ [17]. These interfaces between two insulators have shown even higher 2DEG mobility than before, with an electron density of up to 10^{14} /cm^2. One of the

reasons for the observatuon is the fact that advanced growth and monitoring techniques enable controlled growth of more abrupt two-dimensional interfaces between oxide films. Another is the strong correlation between electrons in transition metal oxides, where the 2DEG was found. The strong correlation between electrons, found in transition metal oxides, is not taken into account by the model of the particle in an infinite potential well. In fact, this model is based on the assumption that the electrons inside the well do not interact significantly.
Because the quasi-two dimensional electron gas (2DEG) in oxide heterostructures has shown unique properties that are promising for applications in all-oxide electronic devices, a huge effort has been made to understand the fundamentals of the behavior of the interfaces.
To this day only some understanding of the fundamental properties and mechanisms have been reached and there is still much work to be done.

4.1.2 Polar discontinuity at interfaces

One of the principle mechanisms that can generate carriers in oxide interfaces is the formation of a polar discontinuity.
An interface can be the one between a bulk material and the surroundings, like vacuum, in which case it is referred to as a surface. An interface can also separate two different materials. In both cases there can be a charge discontinuity at the boundary between a polar and non-polar material. An interface between crystal oxides can thus be continuous and discontinuous from the polarity point of view. Atomic layers, constituting the crystal material, can be alternating positively and negatively charged. While the total charge of the bulk is zero, the interface can still have a polar discontinuity.

An example of such interface is the one between $LaAlO_3$ and $SrTiO_3$. This particular interface exhibits a polar discontinuity. It includes the potential build up in the film, due to polarity discontinuity at the interface. The polarity discontinuity is arising from the neutral ionic charge state in both the $Sr^{2+}O^{2-}$ and $Ti^{4+}O^{2-}{}_2$, continuing into layers in the film with either positive or negative ionic charge state: $La^{3+}O^{2-}$ and $Al^{3+}O^{2-}{}_2$. There are two possible kinds of interfaces Fig.7, either the one where $Ti^{4+}O^{2-}{}_2$ meets the $La^{3+}O^{2-}$ and an access of electrons is obtained or the one where $Sr^{2+}O^{2-}$ continues with $Al^{3+}O^{2-}{}_2$ and an access of dangling bonds are present. (First combination has experimentally been shown to be able to be metallic and conducting and the later one is always insulating.)

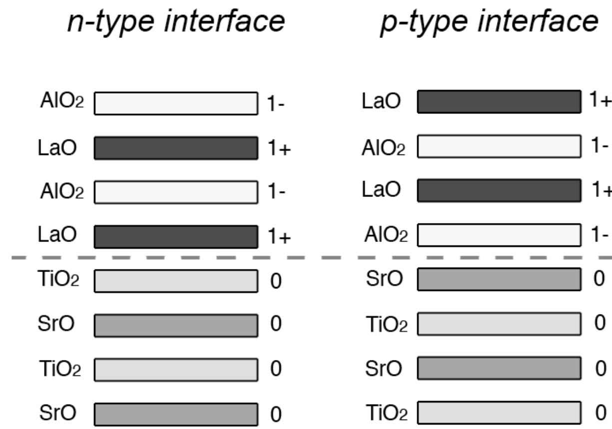

Figure 7: Polar discontinuity model: Schematic of the polar/non-polar interface that arises between $LaAlO_3$ and $SrTiO_3$ – two possible combinations.

Theoretical models of most types of heterostructured oxide interfaces have shown that the resulting charge density is typically ½ electron per unit cell. It is assumed that this charge density is distributed in several atomic layers, near the interface. Correspondingly, transition d subband levels are expected to become partially filled, thus giving rise to electronic states, which are strongly correlated.

4.1.2.1 Polar catastrophe

Ohtomo first proposed an explanation to the 2D conductivity, which includes a compensation of the potential build up, where a charge transfer of half an electron per u.c. from the film is introduced to the interface. The concentration of a 2D electron gas is thereby found at the interface. These mobile electrons are suggested to give rise to the unexpected conductivity. This mechanism was later addressed as a polar catastrophe [18]. According to the model (Fig. 8), with increasing thickness of the LAO thin film the potential builds up.

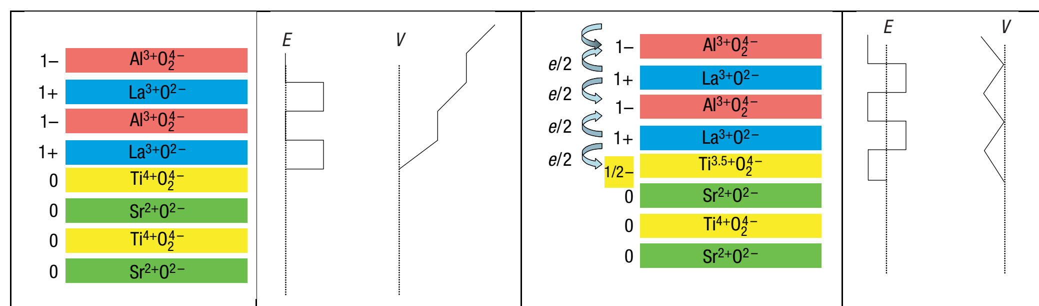

Figure 8: Polar catastrophe illustrated at polar discontinuity interface between Ti-terminated $SrTiO_3$ and $LaAlO_3$; Left: Growing potential in an unreconstructed model. Right: Simple model of electron transfer of half an electron from film to the closest layer of TiO_2, enabling the potential to remain finite.(Nakagawa, Hwang et al. 2006)

Further work on this model suggests that when the potential build-up becomes larger than the energy of the band gap in the $SrTiO_3$, so that the valence band in $LaAlO_3$ reaches higher energy than the Fermi energy, electrons are transferred from the top surface to the interface [51]. This electronic reconstruction model, explaining the conductivity between two insulating materials has drawn a lot of attention, since it provides satisfactory explanation for several observed phenomena, like the critical thickness behavior at 3-4 uc thickness. Experimental results from second harmonic generation [52] support this model and theoretical works have been published with this model as a base [51, 53].

Despite the support from several different aspects, the electronic reconstruction due to polar catastrophe does not manage to provide complete solution that describes all properties of the interfaces. It does not manage to explain the fact that the n-type interface is conducting and corresponding p-type interface is insulating. Furthermore it does not manage to explain the difference between the electronic carrier density in well-oxidized samples and the larger carrier density predicted by the polar catastrophe model.

4.1.3 Oxygen vacancies

It has become clear that oxygen vacancies play an important role for the transport mechanism in oxide heterostructures. It originates from the observation that the conductivity at thin film oxide interfaces is affected by applied oxygen pressure during the growth of the film. Higher oxygen pressure cause worse conductivity and even insulating behavior in $LaAlO_3/SrTiO_3$ [19,27] and films that have been grown at lower oxygen pressures are highly conductive. In addition, it is well known that $SrTiO_3$ becomes metallic upon addition of oxygen vacancies, whereby oxygen vacancies provide free states in the bandgap that donate electrons in the conduction band of the $SrTiO_3$ and result in n-type doping. Annealing after the film deposition at elevated temperatures can lead to the oxygen vacancy depletion.

4.1.4 Doping by cation interdiffusion

An additional mechanism that can generate conductivity at interface between insulating oxides is cation interdiffusion. There are different types of oxides, which can be wide bandgap semiconductors. When they are doped, i.e. addition of other atoms (different elements) that have higher valency, it results in an excess of electrons

into the conduction band and they become conducting. Along the two-dimensional plane, these electrons serve as carriers and can move with high mobility.

A numerous transport studies have been performed and published on the interfaces between $LaAlO_3$ and $SrTiO_3$. Most of them support the electronic reconstruction, which result in 2DEG at the interface. However, intermixing at the film/substrate interface is another suggested possible origin to the conductivity. It suggests that La is doping the $SrTiO_3$ near the interface and similarly to oxygen vacancies causing the n-type doping.
The results from our work on this topic are presented in *"Related papers"*. HAADF STEM is revealing information about the intermixing at the interface at samples grown at both high and low oxygen pressures (information about HAADF STEM in Chp.5). From these results we extracted average intensity profiles across the interface and were able to see evidence of different extent of intermixing for samples grown at different oxygen pressures. Additionally, results on intermixing are supported by MEIS data in [24], where evidence of cationic disorder and phase segregation in $LaAlO_3/SrTiO_3$ heterointerfaces suggest intermixing of La and Sr. The distribution of La atoms at the surface of $LaAlO_3$ approaches better homogeneity with thicker films and reaches stoichiometry between 4uc and 6uc thickness. Moreover, this model is thereby providing an alternative explanation to the insulator-to-metal transition at the critical thickness of 3 to 4 uc, as opposite to the polar catastrophe. Intermixing has also been reported by other authors [54,55].

4.2 Ionic conductivity of nanostructured material

4.2.1 Introduction to microstructure aspects

Recently the interest in combining materials with different functionalities have attracted a lot of interest due to the progress on epitaxial thin film heterostructures. The combination of such materials manage to achieve enhanced effects and unexpected properties, like combining similar structures of $LaAlO_3$ and $SrTiO_3$. In many other cases the desired properties could be enhanced by combining dissimilar materials with different structures and large mismatch parameters.
Increasing the ionic conductivity of solid electrolytes, like in the case of thin film YSZ, is of essential interest. Therefore, effort has been put on trying to understand the mechanisms introduced in the nanostructured materials.

4.2.2 Grain boundary contribution

In the previous chapter, the effect of grain boundaries was briefly mentioned, as a possible path for charge carriers in polycrystalline ionic conductors, where the mobility of the charge carriers can differ from the surrounding alternative paths. It is assumed that the enhanced diffusion for materials with misaligned grains originates from the high ratio of displaced atoms (defects) with corresponding strained bonds that exist in the boundary regions. The result is thus a grain boundary region with high defect density and excess of free volume for high mobility. However, the establishment of this theory is still poor, with reports of contradictory results.

One could imagine that there are different possible paths for ionic diffusion in polycrystalline materials, i.e. along the grain boundaries and across the grain boundaries. The boundaries lying perpendicular to the flow current are usually assumed to block it, thus explaining the cases where the overall conductivity decreases as the grains become smaller. It is however difficult to find information about all aspects and a general agreement in the literature.

The role of internal interfaces, i.e. grain boundaries can be divided in two cathegories called “Trivial size effect” and “True size effect”. The first one refers to the decrease of the grain size in nanostructured materials, which leads to a significant increase of grain-boundary fraction related to the entire volume. It was pointed out that the grain size reduction, might lead to an enhancement of the ionic conductivity through grain boundaries, due to therein existing charging effects [56,57,58,59].

True grain size effect refers to the space-charge layer at grain boundaries, i.e. local physical property modification of the grain boundary region [56,57,58,59]. According to this model, there is a compensation of the grain boundary charges by the formation of space charge in the adjacent grains. The defects in the vicinity of the grain with same charge as in the boundary will be depleted and the opposite charge will accumulate in the space charge region. This region is located in the grain, just next to the grain boundary interface. The extension of this space charge region is given by the Debye length, L_D, and is typically of the order of few nanometers. Calculations on this matter [57] reveal that such accumulation of the charge should lead to enhanced conductivity of the nanostructured material, due to overlapping space-charge regions. More precisely, if the grain size is smaller than $4L_D$ the potential at the grain boundary is enhanced as well as the charge-carrier accumulation. However, if the grain size is larger than $4L_D$ the potential at the grain boundary is not affected. The true role of internal interfaces in YSZ is still to be established.

4.2.3 Charge carrier mobility along the interface between nanostructured film and substrate

Part of the reports on the increased lateral ionic conductivity of thin YSZ films, as compared to the values for bulk, indicates that the contributing factor can be attributed (at least partly) to the film/substrate interface.

Chemical reactions and interdiffusion between films and substrate materials are promoted by the elevated temperatures during the deposition of the films. The electrical transport property of YSZ as well as of $SrTiO_3$ are sensitive to the presence of other elements and this is why it is important to consider this possibility of interaction at the film/substrate interface.
Indications of a possible chemical reaction at the interface between YSZ and $SrTiO_3$ was reported by [43], where EELS compositional analysis revealed some areas containing Zr and traces of Sr simultaneously. It was suggested that cation interdiffusion results in the formation of a $SrZrO_3$ perovskite structure, but there was also a possibility that the observation was just an effect of sample thickness.

Besides the chemical effects, another factor to consider here is that of coherent interfaces between epitaxial electrolyte films grown on single crystal substrate. Factors to consider are elastic strain and formation of extended defects such as misfit dislocations through strain release.
Large, in-plane tensile strain in the YSZ interface layer can create a distortion of the first atomic layers of the YSZ. The ionic transport can thus be affected by resulting disordered oxygen planes at the interface, with more space for the charges in motion.
When the elastic strain is not enough to compensate for the very large lattice misfit, relaxation can occur by the introduction of misfit dislocations at the film/substrate interface. Each dislocation line in such interface can act as a fast transport path.

In summary, there is a possibility that the ionic conductivity in nanostructured solid electrolytes might be a result of both bulk volume and interface conductivity in parallel. Schichtel et.al proposed a model to evaluate the effect of elastic strain on the lateral ionic conductivity, where a ratio between interface and bulk conductivity can be found [60].
However, there is a problem in separating the ionic conductivity from the electronic, which remains to be solved.

5

Experimental methods

5.1 Investigated Samples

5.1.1 $LaAlO_3/SrTiO_3$

Many $LaAlO_3$ thin films, grown on TiO_2 terminated (001) $SrTiO_3$ substrates were investigated using the TEM (a Philips CM200 and a FEI Titan 80-300). All samples were fabricated at the Department of Microtechnology and Nanoscience., Chalmers University of Technology. Films with a thickness of 3 – 8 unit cells were grown using the pulsed laser deposition technique. The in-situ RHEED technique was used to monitor the growth of single layers of ultrathin films during the deposition process. Clear 2D growth of these films was observed from the RHEED oscillations. The films were grown in an oxygen partial pressure of 10^{-2} and 10^{-4} mbar. Electrical measurements show that samples grown at high oxygen pressure are insulating, while low oxygen pressure samples show n-type conductance.

5.1.2 $YSZ/SrTiO_3$ & $YSZ/LaAlO_3$

Different kinds of YSZ samples were investigated for this work. Several TEM samples of each kind were prepared and characterized using mainly FEI Tecnai G2 S-TWIN instrument, operated at 200 kV. These samples were also fabricated as well at

the Department of Microtechnology and Nanoscience, Chalmers University of Technology. The in-situ RHEED technique was used to monitor the growth of thin films during the deposition process. The samples that were grown at low oxygen partial pressure, $1x10^{-6}$ mbar, showed clear 2D oscillations, while other samples grown at high oxygen pressure, $5x10^{-2}$ mbar, showed a distribution of spots typical for a three dimensional rough surface. Attempts were made to perform resistance measurements, using the impedance spectroscopy measurements, at the department of Chemical and Biological Engineering at Chalmers. These have however shown to be inadequate in measuring thin films, since it was not possible to quantify or rule out the impact of the substrate.

5.2 Sample fabrication

Over the past two decades a tremendous progress was achieved in the growth of oxide multilayers, which thereby enabled the extensive research on these systems. The most important steps for this process were the development of film growing techniques like pulsed-laser deposition technique (PLD) and molecular-beam epitaxy (MBE) as well as reflection high-energy electron diffraction (RHEED), used to monitor the growth of individual atomic layers during the deposition process. It also became possible to terminate the oxide substrates at well-defined ionic planes and creating interfaces of choice.

Thin film growth starts with careful preparation of the substrate as well as the target material. The deposition takes place under precisely controlled circumstances. This is crucial since many of the oxides have a very complex phase-diagram and optimization of the deposition conditions, as well as the atmosphere under which the sample afterwards is cooled down, can be a very demanding task.

In-situ reflection high-energy electron diffraction (RHEED) is used to monitor the film growth during the deposition process. The technique is based on the surface diffraction of electrons on the sample. AFM is finally used to study the details of the surface morphology. These methods for characterization are described more in detail later in this chapter.

In this thesis work the $SrTiO_3$ serves as substrate material in most cases, but also $LaAlO_3$ is used. Since understanding of the interface mechanisms obviously involves surface atomic arrangements, knowledge about the substrate surface termination prior to film deposition is crucial. While $LaAlO_3$ has been shown to be a tricky task to discern the termination for [61], the $SrTiO_3$ is well controlled.

Single termination is obtained by a special treatment consisting of chemical etching and annealing [11,61]. The etching process takes place in an aqueous environment and the anneal step in 1 bar of flowing oxygen after which the crystals are kept at ambient conditions before being used for thin film growth.

$SrTiO_3$ substrates are well known to be very sensitive to the temperature and pressure conditions. During the film growth even slight differences in the procedure of heating and cooling can cause totally opposite conducting behavior of $SrTiO_3$. The same sensitivity applies to interdiffusion at the interface. Therefore, it is of crucial importance that the substrate treatment remains the same during this process for all treated samples. Even at the same growing conditions, different laboratories have shown a variation of structure and composition at such interfaces.

5.2.1 PLD

Pulsed Laser Deposition (PLD) is a thin film deposition technique, which can provide stoichiometry transfer from the bulk target to the deposited film, resulting in sharp, well-defined interfaces. An important advantage is the possibility to control many parameters during the deposition process, which have crucial influence on the film properties. Molecular Beam Epitaxy is another technique, which is often used for film growth, but it lacks the possibility to add gases into the chamber during the deposition. This possibility is of crucial interest since low oxygen pressure is usually required to incorporate oxygen into the material in order to obtain the desired phase of the film.
During PLD a laser beam is focused onto a target material, which is than vaporized into a plume by these high power pulses, before it forms the thin film onto the usually heated substrate, Fig. 9. Another advantage with PLD is that it provides very smooth surfaces of films, compared with other film deposition methods. The reason is the varying rate with which the particles arrive to the substrate surface. This enables the deposited material to find the most energetically favorable position in between the pulses, thereby enabling to grow atomically flat unit cell layers.

The process starts with laser beam pulses that irradiate and vaporizes the bulk target surface material into the surrounding vacuum in the form of a plume. This dimension is also dependent on the laser wavelength, the index of refraction of the target material and the pressure inside the chamber.
The plume material re-condenses on top of the typically heated substrate, for a faster and defect free formation of the film. The film growth depends on factors like energy, density, background gas pressure, ionization degree and type of the condensing material. In turn, they affect the surface mobility of the adatoms, which diffuse over the surface until finding a suitable stable position to stick to, constituting a newly formed film.

The three most commonly occurring growth modes are “Layer-by-layer growth”, “Step flow growth” and “Island growth”, amongst which the Layer-by layer growth was used for this thesis work.

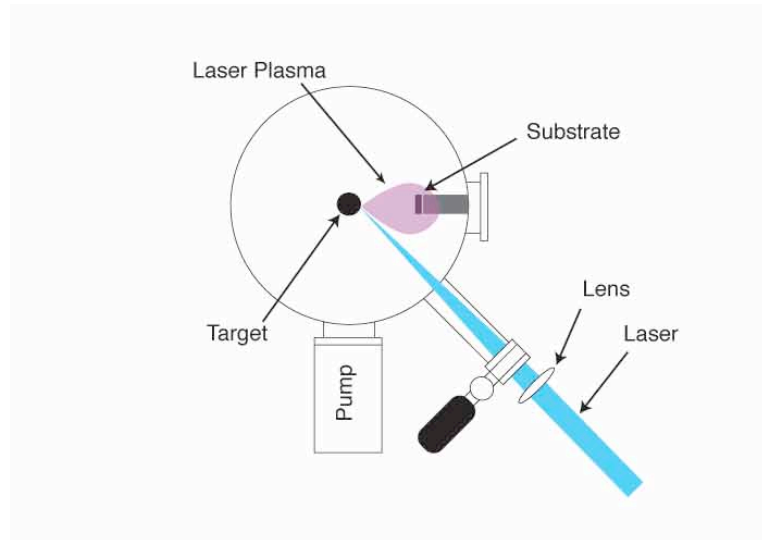

Figure 9: Schematic of a typical pulsed laser deposition system, including the vacuum chamber, pulsed laser beam, quartz lens, substrate and target material. There is also a small oxygen inlet, allowing for control of the oxygen pressure into the chamber (not shown in the figure).

5.2.2 RHEED

The reflection high-energy electron diffraction (RHEED) technique is used to characterize the surface of crystalline materials. Due to a low grazing angle of the incoming beam, the geometry of this technique is convenient for in-situ observations of diffraction processes, while material is being grown. RHEED can measure the atomic layer growth of Pulsed Laser Deposition (PLD) or Molecular Beam Epitaxy (MBE). Recording of the intensity of a specific reflection during deposition as a function of time, provides information about the evolution and mode of the growth. When 2D layer-by-layer growth is achieved, a clear oscillation is seen in the plot with one period representing the completion of one monolayer.

When recording an RHEED pattern, an electron gun generates a beam of electrons, which strike the sample at a very small angle relative to the sample surface. Since the component of the incident electron momentum normal to the surface is very small, the penetration of the electron beam is small. This enables surface specific information, since only the few lattice planes closest to the surface are causing the scattering. A small fraction of the diffracted electrons interferes forming rod-like patterns on the fluorescent screen, located on the opposite side, see Fig. 10. The resulting RHEED

pattern intensity reveals information about the topography of the sample. The rodlike pattern can be observed for perfectly flat and crystalline samples, while samples with surface features, like polycrystalline samples can add complexity to the pattern. Island-like growth cause the amplitude of the oscillation to decay, thus the intensity variation disappears from the RHEED patterns.
The electron energy of the incoming beam is important, since a high energy results in a decrease of surface specificity and forward scattering then becomes more important. Usually high energy electron beams are used of around with energies of 3-100 keV.

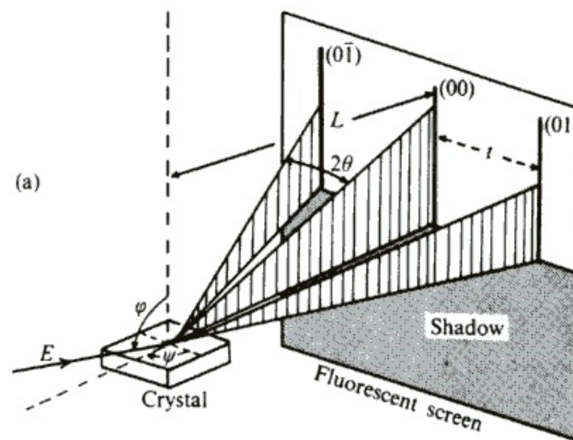

Figure 10: Schematics of the experimental setup in RHEED. The component of the incident electron momentum normal to the surface is very small and thus the penetration of the electron beam is small. The Ewald sphere cuts the (00) rod almost along its length, resulting in long streaks normal to the shadow edge of the sample.

5.3 Electrical characterization

The most suitable technique to use for electrical characterization of homogenous thin films is the so-called Van der Pauw technique. It is a commonly used method for samples with approximately two dimensional geometries, like in this case, as it allows measuring the sheet resistivity, sheet carrier density, doping type and carrier mobility. The basic principle is to use four simple ohmic contacts placed as far as possible from each other. The Van der Pauw method then allows measuring the sheet resistance R_S according to the setup in Fig. 11a in combination with the equation (5.1). In the general case solving equation (5.1) for R_S require numerical methods; however the

solution is trivial if $R_a \approx R_b$ (Isotropic case), condition verified in all measured samples. The sheet carrier density n_S is then obtained from the setup according to Fig. 11b, where the Hall voltage V_H is measured.

a) b)

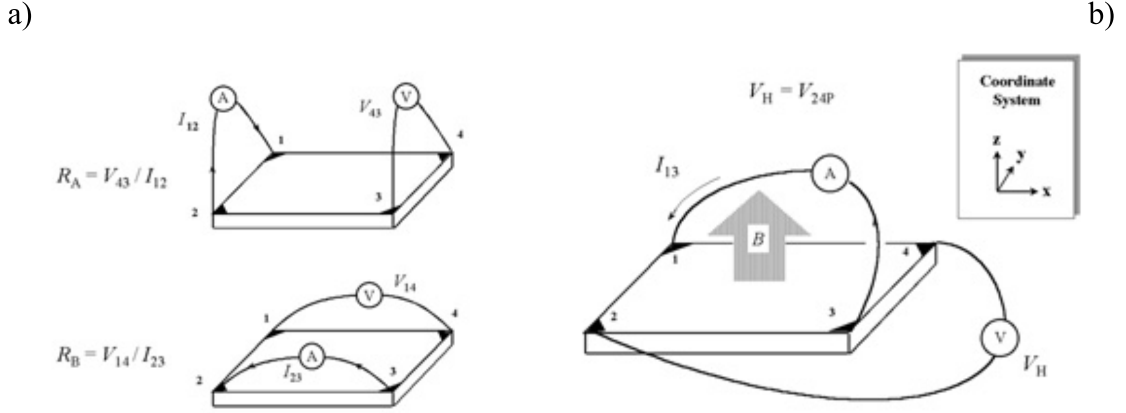

Figure 11: Schematics of a four-point Van der Pauw configuration.

$$\exp\left(-\frac{\pi R_A}{R_S}\right) + \exp\left(-\frac{\pi R_B}{R_S}\right) = 1 \qquad (5.1)$$

The use of four-point probe in the Van der Pauw measurements, as compared to the simple 2-point probe method, provides the advantage of neglecting the additional resistances from the contacts between the measured material and the probe. The two extra probes are used to measure the voltage potential of the material surface, while carrying very low current and thus disregarding the unwanted voltage drop from the contacts.

In the case of the conducting interface of LAO/STO, it is assumed to be 2 dimensional and surrounded by two oxide insulators. This fact automatically raises some questions regarding the measurement of this electronic conductivity, regarding contacting and accuracy. Several working contacting methods have been reported in the literature. In the case of the LAO/STO hidden conducting layer, use of sputtered gold pads on top of the Ti adhesion layer of the thin film surface has been shown to work satisfactory.

5.4 Structural Characterization methods

5.4.1 AFM

Atomic Force Microscopy (AFM) belongs to the Scanning Probe Microscopy (SPM) family, which is a branch of microscopy that forms images of surfaces using a physical probe that scans the specimen. The probe is swept, line by line, over the sample surface, recording the probe-surface interaction as a function of position. AFM measures the force interactions between the atoms in a sample and a probe, which are usually designed as cantilevers with integrated sharp tips. In this way sample surfaces at the subnanometer scale can be measured and atomic resolution is achieved. The AFM does not require an electrically conductive sample, which enables studies of all materials without any specific surface preparation. The shape of the sensing tip at the end of the cantilever, as well as the detecting sensitivity of the system, is limiting the lateral resolution of the AFM.
There are three common AFM modes: non-contact-, tapping- and contact-mode, and in this work the investigations have been performed in the tapping mode.
Here the cantilever is driven to oscillate up and down at or near its resonance frequency (oscillation amplitude is 10-100 nm) by a small piezoelectric element mounted in the AFM tip holder. Piezoelectric elements that facilitate tiny but accurate and precise movements on (electronic) command enable the very precise scanning of the tip. Due to the interaction of forces acting on the cantilever when the tip comes close to the surface, the attractive van der Waals force, for large interatomic distances, or the repulsive electrostatic forces, cause the amplitude of this oscillation to change with an amplitude-shift as the tip gets closer to the sample. This change of the amplitude (and the phase) is than recorded with the help of a laser and a detector (photodiode), according to the figure.

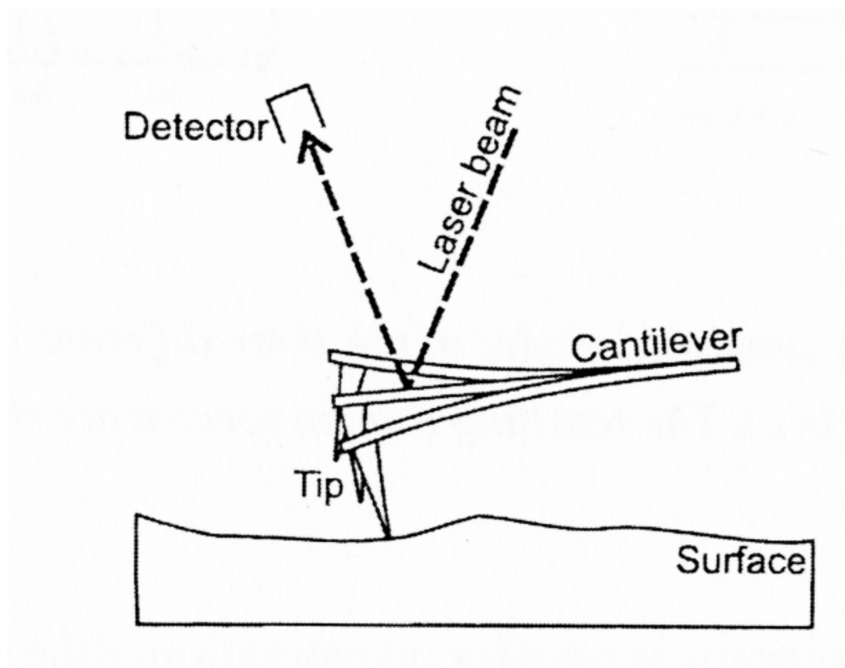

Figure 12: Simplified schematic figure of the general setup of a tapping mode AFM. The tip on the cantilever oscillates while being scanned over the investigated surface. The tip position is detected with the help of a reflected laser beam [62].

5.4.2 X-Ray Diffraction

X-ray diffraction (XRD) is mainly used for phase identification and crystal structure determination including the unit cell parameters. It can also be used to estimate the size distribution of the grains.
XRD is based on the constructive interference of monochromatic X-rays (specific wavelength λ) interacting with a crystalline sample. The production of X-rays is based on the principle where a metal target, usually Cu, decelerates and is ionized by a beam of high energetic electrons thereby generating x-rays. The interaction between the x-rays with the crystal may be described as follows: a regular atomic arrangement in a material produces diffracted waves with a certain direction, according to Braggs law: $\lambda = 2d_{hkl}\sin\theta$, Fig. 13. Here the wavelength λ of electromagnetic radiation is related to the diffraction angle Θ and the lattice spacing d_{hkl} in the crystal.

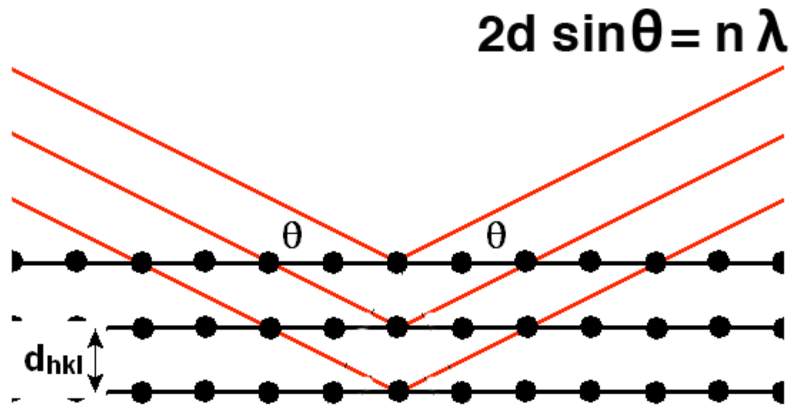

Figure 13: Simple illustration of beam interaction with lattice planes according to Braggs law. Relationship between the radiation wavelength λ, the lattice plane distance d and angle of incidence θ is shown.

Information about a material is obtained in the form of characteristic diffraction peaks in a diffractogram.. To identify the different crystallographic arrangements *(*d_{hkl} interplanar spacing) and orientations of the phases, the intensity of the diffracted radiation can be measured as a function of the angle between the beam and the sample, i.e. Intensity (counts per second) versus 2θ (degree) according to the Fig. 14.

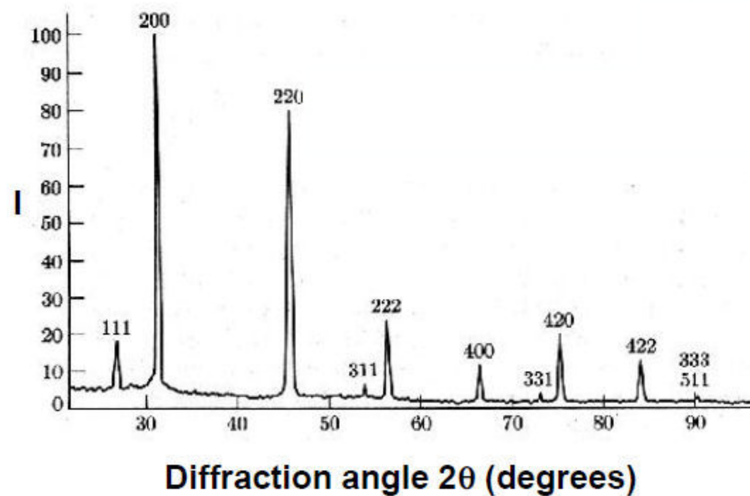

Figure 14: The characteristic X-ray emission spectrum the showing 2θ-ω scan.

5.4.3 *Electron Microscopy*

In a transmission electron microscope (TEM) a beam of electrons is focused on and transmitted through a thin specimen. The electrons interact with the atoms in the specimen as they pass through and undergo diffraction and scattering events. The transmitted electrons are focused to form an image that is magnified prior to being detected by an imaging device, such as a fluorescent screen or a CCD camera. It is possible to resolve as small features as 0,5 Å in size with a TEM, which is sufficient to resolve single atomic columns and opens a new world of possibilities.

The idea of an electron microscope was born by Max Knoll and Ernst Ruska in 1932, only 7 years after Louis de Broglies theory about the wave-like behavior of the electron. The idea was spurred by the need for a higher resolution than achievable by the optical microscope could, where the resolution is limited by the wavelength of visible light, around 400-750 nm. The wavelength of electrons, on other hand, is typically on the order of a few pico meters in a TEM. This is easily calculated using de Broglie relation for accelerated matter, $\lambda = \frac{h}{m_e v}$, where λ is the wavelength, m_e is mass of the electron, v is velocity of the electron and h is Planck's constant.
However, the resolving power of an electron microscope is not directly proportional to the electron wave length, but is also affected by a combination of the aperture size, the so-called lens aberrations and the sample quality.
In the early age of TEM the common believe was that if one only use the optimal focus and manage to reach the resolution limit, it should be possible to image even the weakly scattering atomic columns, such as those consisting of carbon. The theory of that statement was correct, but what was overlooked was the limitation due to the lens aberrations. These are imperfections of magnetic lenses, causing beam rays that pass through the lenses to fail in converging to the same point. Nowadays the main issue for TEM development is correcting for the aberrations and improving the quality of the lens-system and also improving the techniques with which the preparation of the samples is carried out.

As a microscopist one has to be aware of both the opportunities and the limitations of the microscope. A TEM offers a number of different techniques that can be used. They usually have different requirements of the alignment of the microscope and/or the sample quality. Thus, an overview of the techniques used in this work will be given here. Further details about the setup and the alignment of the TEM can be found in [63].

5.4.3.1 TEM setup

A TEM is fully separated from the environment by a column under vacuum. This is necessary to avoid interaction between the electron beam and the surrounding media. The main components within the column are: the electron source that is connected to a high voltage generator, electromagnetic lens systems and a fluorescent screen and/or digital camera.

All lenses in the TEM, consist of coils generating an electromagnetic field. By changing the magnetic field the strength of the lenses is changed and it is possible to deflect or focus the beam as desired. All magnetic lenses are convex – focusing the probe (electron beam) to a point.

The beam that is generated by the electron gun at one end of the column is first passing through a condenser lens system before reaching the sample. After being scattered by and transmitted through the sample the electrons are focused by the objective lens, producing an image of the specimen. The image is further magnified by the projection lens system and is viewed at the opposite end of the column, see Fig. 15.

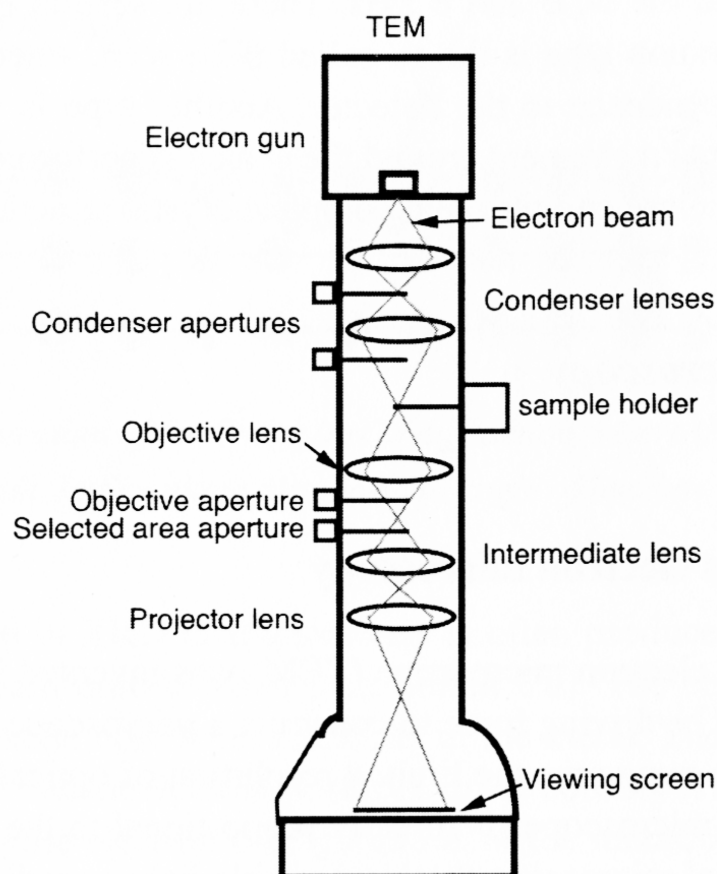

Figure 15:Schematic overview of a TEM setup [64].

Electron source

In the electron gun of the TEM the electron source generates electrons. There are three main types of electron sources in use, tungsten hairpin LaB_6 and the field-emission gun (FEG). The first two are thermionic sources and they use heating to produce electrons while the third one uses an electric field to assist the electrons in tunneling out from the source tip.

The source should be chosen according to the need of the study. All three types of guns offer a good choice for a specific task. One limiting factor is the brightness, the current density of the beam per unit solid angle of the source, which affects the contrast and resolution of the TEM.

Tungsten sources are very stable source of electrons and are the least expensive, but offer lower brightness and also have limited lifetimes. This kind of source is suitable for imaging at magnifications up to 40-50 kX in TEM mode. LaB_6 sources provide a smaller emitting area and up to 10x more brightness than tungsten, but the total beam current is smaller. If the desired magnification for imaging is 50-100 kX, the LaB_6 source will provide the most suitable intensity/brightness. In this work both LaB_6 (Tecnai F20) and a Schottky Field Emission (Titan 80-300) guns are used. For achieving good phase contrast at high resolution, a high spatial coherence is needed and that is provided by the field emission gun. Moreover, a FEG is the best choice for performing the experiments requiring small probes, such as scanning techniques.

Condenser lens system

The beam of electrons generated by the gun is first focused by a condenser lens system. The condenser lens system, helps to shape the beam onto the specimen after desire, for example a parallel beam for TEM or a convergent beam for STEM. It consists of two or more lenses and corresponding apertures.

The strength of the first condenser lens, C1, controls the spot size, which is the minimum diameter of the illuminated area of the specimen. It does so by controlling the magnification of the gun crossover, and thereby it also affects the beam convergence at the plane of the specimen. The second condenser lens, C2, also affects the convergence of the beam, as well as the diameter of the illuminated area of the specimen, by focusing the electron beam directly onto the specimen.

Besides condenser lenses, corresponding condenser apertures are crucial for the quality of the resulting beam. All condenser lenses are equipped with additional condenser lens apertures. These are basically an opening through which the beam travels, cutting away electrons with large convergence angles that suffer more from off-axis lens aberrations. An aperture is simply limiting the current passing through a lens. The smaller the C2 aperture, the more parallel beam is obtained, but also less intensity is passed through.

In most new microscopes there is also a third condenser lens, C3, which is generally used in combination with the C2. Independently of the C2 aperture, C3 allows the beam convergence to be adjusted. This can be very useful in many settings where a parallel beam otherwise would not be possible.

Objective system

The objective lens is considered to be the most important lens of the microscope, because it produces the first image of the specimen. The objective lens is also the lens which suffers most from different aberrations and great concern should be put to align and correct for these aberrations, otherwise the errors will become magnified by the other lenses as well. The objective lens forms diffraction pattern in the back focal plane of the lens. The objective aperture may be used to select the diffraction spots of interest to contribute to the final image, thereby enhancing the contrast in the image.

Projection system

The projection lens system consists of intermediate lens, selected area aperture and a projection lens system, according to the Fig. 15. The intermediate lens can be focused on either the initial image or on the diffraction pattern in the back focal plane of the objective lens, resulting in either an image or a diffraction pattern on the screen. A selected area aperture is used to select a specific area of interest in the image that the diffraction pattern will be studied from. It is placed in one of the image planes in the projection lens system. The main function of the remaining projection lenses is to magnify the image formed by the objective lens.

Aberrations

Aberrations are lens imperfections that cause distortions in the image formation. Rays from a point in the object plane fail in converging to a point in the image plane. There are different kinds of aberrations in optical systems. The three aberrations with highest impact on performance and resolution are astigmatism, spherical aberration and chromatic aberration.
Astigmatism arises when the electrons are deflected and focused by a non-uniform magnetic field. This effect can occur due to lack of perfection when fabricating and mounting the lens pole pieces, as well as from charging contamination introduced by dirt. To take care of this problem, usually a stigmator is used, which is a part of the routine for aligning the microscope for atomic resolution imaging.
Spherical aberration can usually, unfortunately, not be corrected for in a simple way, through an alignment procedure or specimen preparation. It is an effect of the magnetic lens field failing in bringing both on-axis and off-axis rays to a focus at one

point somewhere along the axis. Apertures placed above the lenses limit the electron rays incident with high angles and in that way reduce the effect of spherical aberration somewhat. To further reduce this effect is a harder task. Nowadays the more advanced microscopes are equipped with aberration-correctors, which dramatically improves the resolution of the microscope [65,66]. Aberration correctors are constructed of a series of finely adjustable lenses to compensate for spherical aberration. C.L. Jia and co-workers [55,67], for example, managed to enhance the contrast in the HR-image, using negative spherical aberration (positive spherical aberration in combination with an underfocus), thereby succeeding to image even the weakly excited atoms.
Chromatic aberration, on the other hand, arises when the electron beam is not perfectly monochromatic after passage through the specimen. Using thinner specimens and the so called C_c corrected microscopes can reduce the effect of chromatic aberration.

5.4.3.2 Imaging

Images in the TEM consist of small areas with different amount of intensity, building up the contrast. Thus contrast is the main information carrier. There are different types of contrast to be used when acquiring images in a TEM. The choice depends on the material to be investigated as well as on the desired information.

When electrons are transmitted through a specimen, they interact with the atoms in the specimen in different ways, depending on the atomic number, Z, the mass or the density ρ and the thickness of the sample. There is logically a higher probability for scattering with heavier atoms, as well as with thicker specimens. Also the atomic arrangement, i.e. the crystal structure, has an effect on the scattering. The diffraction pattern shows the redistribution of scattered electron intensity, which for a crystalline sample is a spot or ring pattern. This may be used for modifying the contrast in the image.
Amplitude contrast is obtained by choosing only certain diffracted spots or the transmitted spot in the diffraction pattern before switching to image mode. The objective aperture can be used to form either bright field (BF) or dark field (DF) images by selecting the direct or scattered electrons, respectively. This offers the possibility to easier distinguish information of different kinds. Selecting one or several diffracted spots will increase the image intensity from crystals whose atomic planes are oriented in such a way that they fulfill the Bragg condition and scatter to the diffraction spots. Those regions will appear bright in a dark surrounding area in a DF image.

BF imaging is enhancing the contrast between thinner and thicker areas of the sample, or between regions containing lighter atoms and their corresponding neighbours with higher Z elemental composition. This type of contrast is called *mass thickness*

contrast. It is mainly used for noncrystalline specimens, i.e. amorphous, like polymers and biological materials. Using the objective aperture to choose between the direct or the scattered beams allow for contrast enhancement of amorphous materials as well. The size of the objective aperture is also important in the sense that it allows for choosing how strong contrast variations will be seen in image. An image without the aperture will show poor contrast, due to the contribution of a large number of beams.

Diffraction contrast, another form of amplitude contrast, is obtained from crystalline samples and is the main contrast source for BF/DF imaging. It is governed by scattering of electrons by the crystal planes, fulfilling the Bragg condition. For different orientations between the electron beam and the diffracting crystalline planes, there will be a variation in the number of the diffracted electrons. This will result in an image with a brighter contrast region against the darker surroundings for DF imaging and vice versa for BF imaging. In a BF image, areas that appear dark correspond to areas where the Bragg condition is fulfilled for certain atomic planes, along with reduced direct beam intensity. For the same reason, this technique is useful when imaging lattice strain, bending and defects.

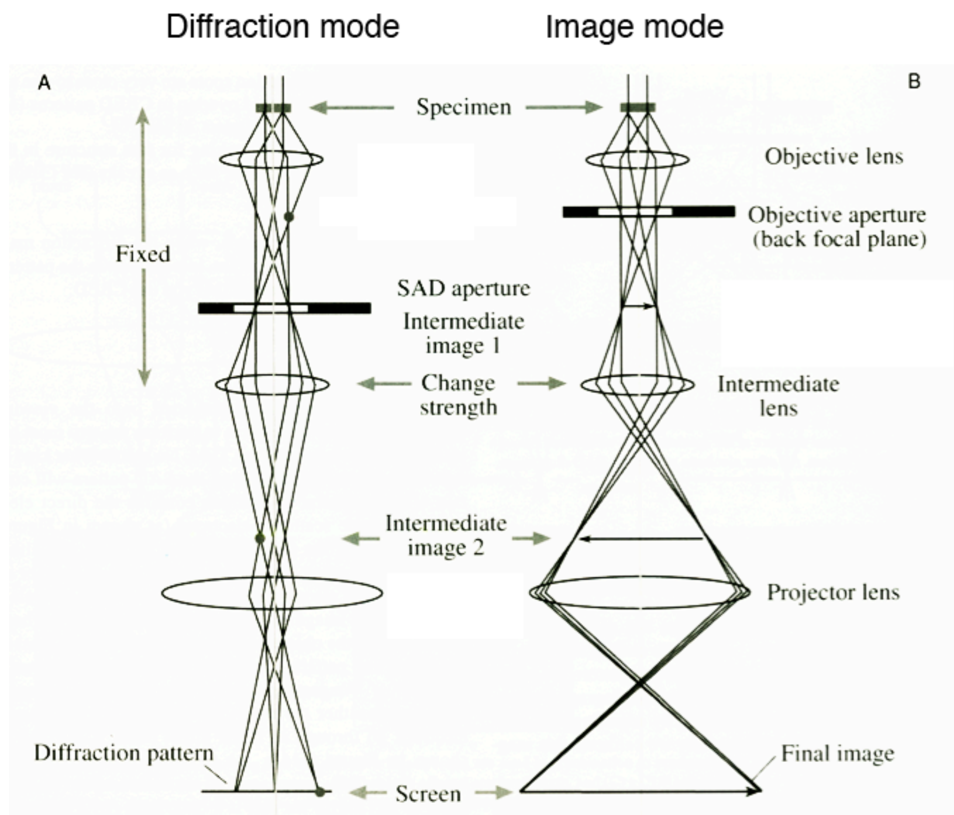

Figure 16: Schematics of the ray diagram of electron beam path through the column of a TEM lens system in diffraction mode (left) and image mode (right).

There are also other types of contrast, like phase contrast and Z-contrast. These will be treated next, in more detail.

5.4.3.3 HRTEM

High resolution TEM is all about *phase contrast*. Phase contrast is obtained from the interference between the direct beam and one or more phase shifted diffracted beams. In contrary to BF and DF, a phase contrast image is obtained by selecting more than one diffracted beam for formation of an image. The image contrast is built up by the so-called fringes, which are visible as alternating bright and dark lines with certain periodicity. However, it is important to remember that these fringes are not directly interpretable into atomic planes. The phase contrast is sensitive to many factors including focus of the objective lens, sample thickness, crystal orientation, scattering factor as well as changes in the astigmatism.
There are three kinds of fringes, that build up the phase contrast of HRTEM and those are lattice fringes, Fresnel fringes and Moire fringes.
Lattice fringes are, as the name reveals, originating from the interference of the mutually phase shifted beams from each lattice plane with the direct beam. These fringes thereby have the same spacing as the lattice planes and valuable information about the structure of the sample is obtainable. The intensity from the transmitted beam in combination with the lattice contrast is what we can observe in a HRTEM image. A certain position with higher intensity in the image is however not directly coupled to a specific position of the atomic columns, since the intensity is a result of both phase and the amplitude of all beams building up the image. The phase can cause shift of contrast, as a consequence of the interaction with the sample. This can occur with change of thickness, focus, orientation or aberrations.

Moire fringes are appearing from the interference of two overlapping sets of lattice fringes. The two sets have either different orientation or spacing and can be used to calculate the mutual orientation relationships.

If the sample is not focused, *Fresnel fringes* will appear along the sample edges and interfaces, caused by the phase changing the contrast in those areas. These fringes are very useful when working with the HRTEM, since they are indicators of the relative position of the focus plane and sample. When the number of visible Fresnel fringes is decreased to zero, the sample is in perfect focus, the and overall contrast from the sample is decreased.

5.4.3.4 Electron diffraction

Diffraction in electron microscopes is based on the same basic principles as in other diffraction techniques. Waves of different kinds interact with matter, such that the waves bend and spread around small openings, following Bragg's law. This effect is mostly pronounced when the wavelength of the wave and the opening of the object have roughly similar dimensions.

In electron diffraction the wave nature of electrons interact with matter having a periodic structure, resulting in interference patterns that give information about the atomic arrangement within the solid. This makes it a very well suited technique for studying crystal structures. The periodic structure of a crystalline solid acts as a diffraction grating, scattering the electrons in a distinct pattern of constructive and destructive interference. Constructive interference occurs when the electrons scatter at the Bragg angle. The result is the diffraction pattern from the crystal, which mathematically corresponds to a Fourier transform. Observation of such a diffraction pattern yields information about the symmetry of the repeating unit of the structure, the unit cell, and the size and shape of this cell, see Fig. 17.

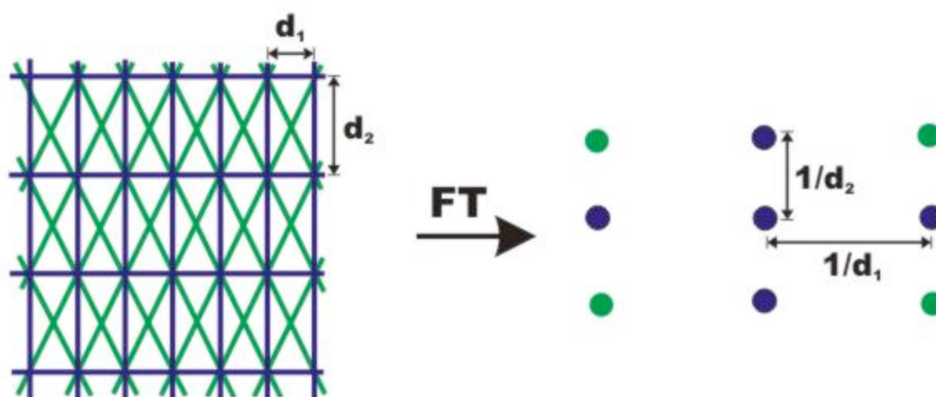

Figure 17: Schematic model showing the relationship between image and diffraction pattern of a repeating structure, representing a crystalline grating.

Considering the relationship between the wavelength of electrons and the lattice fringes in a crystal it becomes clear why we need an electron microscope to "see the atoms", and why the optical microscope is not enough. Hereby the condition for elastic scattering (the Bragg equation $n\lambda = 2d\sin\theta$) is satisfied and diffraction will occur. Each set of parallel lattice planes is represented by spots in reciprocal space (diffraction pattern). The spots are separated by a distance of 1/d from the origin and they are perpendicular to the reflecting set of lattice planes. A shorter interplanar distance between two set of planes in a crystal results in spots that are further away from the direct beam in the diffraction pattern.

As mentioned before, a TEM can be run in image or diffraction mode, depending on the strength of the intermediate lens, shown in Fig. 16. In diffraction mode the projection lens system is aligned such that the back focal plane of the objective lens, where the diffraction pattern is first obtained, is imaged on the screen. Thereby we obtain a 2D reconstruction of the reciprocal lattice of the sample. The reciprocal lattice is actually a 3D array of points, whose intensity becomes visible on the screen when the so-called Ewald sphere intersects them. This happens only when the Bragg condition is fulfilled. The Ewald sphere is an imaginary sphere, which describes the relationship between the wave vector, k, of the electron beam, the diffraction angle θ for a given reflection and the reciprocal lattice of the crystal. The length of the vector k is proportional to the electron energy and it represents the radius of the sphere.

Tilting the incoming beam in relationship to the sample, tilts the Ewald sphere in reciprocal space. The outcome is that different sets of planes are fulfilling the Bragg condition and can therefore be imaged. The possibility of tilting the sample in the TEM is therefore of crucial value.

A huge advantage of electron diffraction in TEM is the possibility to distinguish information about the structure from a very small region of the sample. This can be done by using selected area electron diffraction (SAED) or convergent beam electron diffraction (CBED).

As mentioned earlier, SAED is obtained when the selected area aperture is inserted into the intermediate image plane, whereby it is possible to select a specific region of the sample that will cause the diffraction onto the screen. This technique is usually applied in the parallel-beam TEM mode.

CBED however can be used to obtain diffraction patterns from even smaller areas, than is possible by SAED. It can offer information about the fine structure. Here a convergent beam is used for illumination of a tiny area of the sample. Improved spatial resolution is not the only advantage. In addition, CBED can give additional information about the specimen, like the thickness and more precise unit cell and lattice parameters determination.

5.4.3.5 STEM

STEM is used for imaging and chemical analysis of specimens. The working principle is that a focused beam of electrons is scanned over a very small area of the sample and an image is built up. STEM in the TEM (as opposite to SEM) is used on thin samples, which allow for collection of the transmitted beams. There are different detectors, which can be inserted for collection of different information, Fig. 18. They record the magnitude of electron scattering from each point of the sample.

The idea of a STEM came in the late 1930s, but it was not before the 1970s that the technique became more used, in connection with the first combined TEM/STEM microscope, Philips EM200. Today there are both combined TEM/STEM microscopes, as well as dedicated STEMs.
When using STEM the electron beam is focused to a small probe of the order of around 1 Å in diameter and scanned across the sample. The resolution limit is directly connected to how small probe size can be obtained. However, the brightness that depends on both the current density per unit area and on the incoming angle, is strongly affected as well, according to the relationship $B=I/(\pi A\theta^2)$, where B is the brightness, I is the beam current, A is the beam area and θ is the illumination semi angle. Directly below the sample in a back focal plane different annular detectors can be inserted according to the figure. The transmitted beam can be used with the BF detector so that the background/holes appear bright.
When the annular dark field (ADF) detector is used, it can be changed so that the inner angle of the detector collects scattered electrons at different angular range. In this way different information can be gathered depending on if only the high angle scattering is collected (HAADF) or if also a contribution from low angle scattering is forming the image (LAADF).
In the past 15 years impressive progress have been achieved regarding the correction of the major geometrical aberrations of the probe forming lenses. This has improved the resolution in STEM by more than a factor of two, which allowed for the first direct image of a crystal showing sub-Ångstrom resolution (0,78Å) [68].
The main advantage of high resolution STEM imaging using the HAADF is that the high angle scattered electrons contribute to form a Z-contrast image. It makes it possible for the user to directly relate the contrast to atomic positions and chemical composition. This contrast will be discussed further in next section.

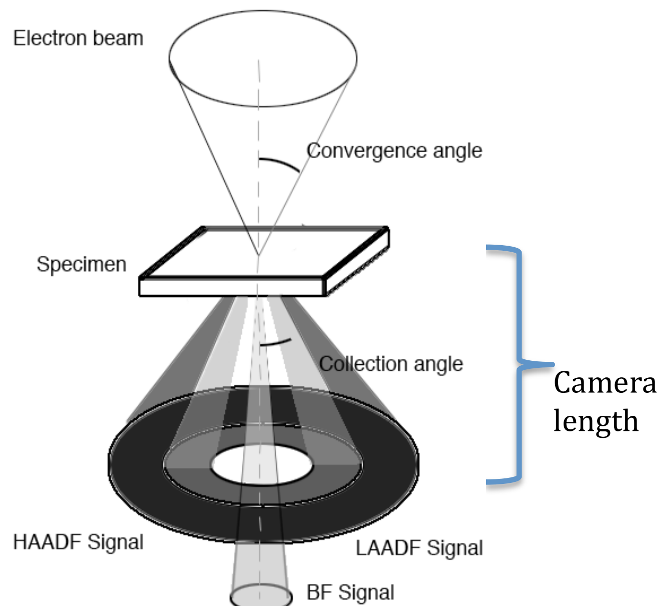

Figure 18: A schematic figure showing the symmetry between the interacting electron beam and the different detectors used for acquiring STEM signal.

5.4.3.6 HAADF STEM

HAADF STEM analysis can be performed to extract information about the structure of a specific material. An HAADF detector collects transmitted electrons scattered at high angles forming an annular dark field image. The high angle of scattered electrons is desired since those electrons have been scattered close to the atom sites (approx. within 0,1Å). This small distance is comparable to atomic vibration amplitudes, and thus the intensity at high scattering angles is dominated by Thermal Diffuse Scattering (TDS), according to Einstein's model of independently vibrating atoms treated as harmonic oscillators [69].
During STEM imaging the HAADF detector is located at a back focal plane and the collection angle can be varied by varying the camera length (see figure).
The intensity of those incoherently scattered electrons increases with the atomic number Z and a dependence of Z to the power of between 3/2 to 2 (depending on the collection angle) is claimed for the electrons scattered at high angles [70]. Thus atoms of heavier elements appear brighter than lighter.

In a TEM the sample is tilted to a zone-axis of the sample, so that the electron probe is oriented exactly along the atomic columns. Thus each intensity spot corresponds to one atomic column, giving rise to atomic number contrast in a HAADF STEM. Performing a simple calculation suitable scattering angles can be estimated, making sure that the intensity in HAADF STEM images is free from strain effects. From this we know that if we use scattering angles higher than a certain angle for a specific material, we can be sure to only mainly receive information from the incoherently scattered electrons. This result is received by carefully choosing the suitable camera length [71].

The inner detector angle θ_1 should be chosen so that

$$e^{-2M_K s^2} \leq 0,02 \tag{5.2}$$

This ensures that no matter what the crystal orientation, the image is dominated by TDS, where $M = 8\pi^2\bar{u}^2$, $s = \theta_B/\lambda$ and $\bar{u}^2$ = mean square vibration amplitude.

Effect of electron channeling

Channeling of the electron probe as it propagates through the sample play an important role for the formation of the HAADF image [72]. The effect of charged particle propagation through a crystal along a low-index direction, without significant scattering angle is called the *Channeling effect*. This means that the electrons that are scattered by atoms in the specific column are more likely to continue its way through the specimen along the low index direction, as long as the atomic columns are oriented along the incident beam. In this case, according to [73] the probe is not spreading enough while it propagates through the sample, so that it does not interfere with another neighbouring atom. This is especially true for single crystal perovskite oxides, due to their large lattice constant. Apart from the orientation of the crystal, the channeling effect varies with the type of atomic species. Upon beam propagation through two equal crystals, containing different species, the beam can channel significantly different distance along the atomic columns [74]. This effect image interpretation considerably, which brings us to the next topic, concerning the sample thickness.

Effect of sample thickness

Sample thickness has shown to give a high contribution to the image contrast in ADF STEM images [73]. The main effect of an increase in sample thickness is the increase of the background intensity, which also lowers the intensity contrast. However, the contribution of the background intensity is equal to the intensities of the atomic columns and the channels between them. If the background is subtracted from the signal, the quantitative interpretation of image contrast in terms of atomic number contrast is obtained and maintained.
Since the channeling effect is different for columns occupied by different species [73,75], and thicker samples tend to spread the beam more, contributing to a higher background intensity, it is obvious that the thickness has a crucial effect on the image contrast.

Another important aspect is the chemical nature of the atoms and their contribution to the background signal. As the TEM foil thickness increases, the background intensity in heavier materials rises more rapidly than in lighter, possibly making the analysis of the heterostructures more complicated. This also causes the background intensity at an interface to be intermediate between that of the light and heavy crystal. However, keeping the area of investigation thin can minimize this effect.

Oxley et al studied the evolution of the ADF signal as a function of specimen thickness [73]. They were able to show that a relatively small change of thickness of the sample does not change the interpretation of the signal significantly. Furthermore, according to the simulations of $LaMnO_3$, the intensity changes significantly for the

thickness range of about 20 – 100 Å, but when the thickness passes 100 Å, further increase of the thickness does not effect the interpretation of the signal. The later applies to the samples for a range of the thicknesses that are usually obtained experimentally.

Finally we can conclude that due to these effects it is crucial to make sure that as thin samples as possible are used for the investigations.
Determination of the thickness is performed using the thickness mapping. This is done using energy filtering, by acquiring a ratio between the zero loss signal and the total intensity of the EELS spectrum. This results in a thickness map, where the pixel intensity is proportional to the mean free path of the sample (λ). λ is the average distance that the electron travels between scattering events and is specific for a specific material. Thus, from the obtained value of the mean free path it is possible to estimate the thickness of the sample.

Effect of amorphous layer

Most often there is a layer of amorphous material covering the surface of the crystalline specimens to be investigated in the TEM. The presence of such an amorphous layer can, depending on its thickness, strongly decrease the contrast from the atomic columns in ADF STEM. There are various reasons for the presence of such amorphous layers. Most often they are a result of the preparation techniques of the TEM specimens, where the requirement of thin, electron transparent samples is crucial. To achieve such thin crystalline specimens, techniques like manual polishing and ion milling are most common, which usually result in the creation of amorphous material on the surfaces. The thickness of these layers is however varying, depending on the technique setup as well as on the operator. Cleanliness of the sample as well as of the instruments used are crucial in order to minimize the effect of re-deposition of unwanted material during the instrumentation. However, the complete understanding on the effect of the presence of the amorphous layers on the ADF-STEM imaging is still not reached.

Mkhoyan and co-workers [76] used multislice image simulations to study the effect of amorphous layers present on the surface of TEM specimens on the ADF STEM imaging, both in uncorrected and aberration-corrected STEMs. Their analysis is based on a sample that is covered with amorphous layers on both surfaces and show the following results: Parts of the beam that have travelled through the first amorphous layer are broadened, i.e. scattered to larger angles, creating a Gaussian background. The Gaussian background becomes broader with an increase in the thickness of the amorphous layer. The rest of the beam passes without any alteration, but it suffers from loss of spatial resolution, due to a change of focus when it reaches the crystalline part, corresponding to the thickness of the amorphous layer. Depending on if an aberration correction system is used, the sensitivity to defocus varies and little or no

contrast can be resolved. However, with appropriate changes in defocus value specimens with amorphous layers on the top (beam entry surface) can also be imaged and high- resolution ADF images with substantial contrast of atomic columns can be obtained [76]. The type of the amorphous layer varies with atomic weight and stronger background is caused by heavier elements. It is however, still not completely clear what are the boundary limitations on the ADF STEM due to the presence of the amorphous layers.

5.4.3.7 Energy-dispersive X-ray Spectroscopy (EDS)

Chemical analysis in TEM can be performed using the X-ray signals. In a TEM the X-ray photons are generated upon interaction between the electrons of the incoming beam and the core electrons of the atoms in the sample.

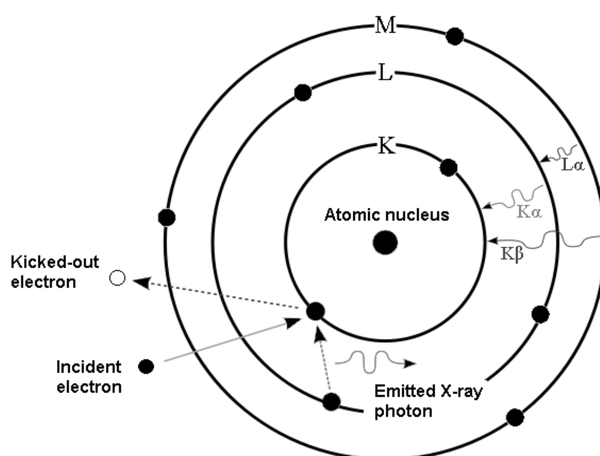

Figure 19: Bohr atomic model explaining electron absorption and x-ray photon emission.

Incoming electrons can knock out a core electron from an atom in the material of interest, whereupon another electron from an outer shell takes its place. From each of these processes there will be an x-ray photon emitted, with a specific energy corresponding to the difference between the atomic energy levels of the target atoms. The Bohr model in Fig. 19 describes these frequencies. The resulting characteristic X-ray photon is detected by a specific EDX detector, which is mounted above the specimen in a TEM. The specific energy difference between the states of the element allows the chemical analysis.

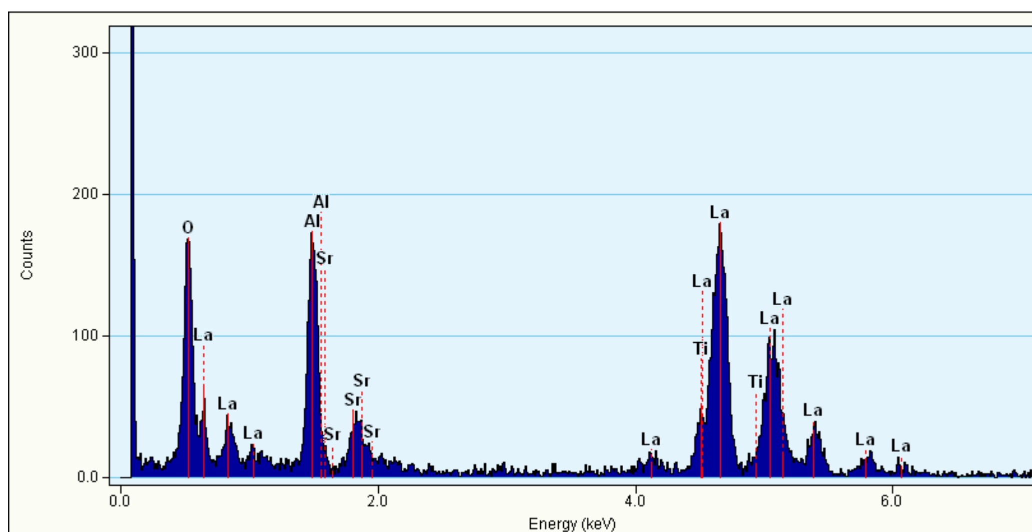

Figure 20: Typical EDX spectrum display showing energy peaks at different energies, corresponding to the difference between characteristic energy states of specific elements.

EDS allows for both qualitative and quantitative analysis of a material, whereby parameters like atomic number of the containing elements, the absorption effect and the overlapping peaks, need to be taken into account.
EDS can be used for chemical analysis in both SEM as well as in TEM, but the benefit here is that a thin TEM specimen naturally limits the interaction volume, improving the spatial resolution of the signal. Another benefit is that the use of a thin specimen limits the absorption effect. There are however other effects to be aware of when acquiring EDS in TEM, like the tilt of the sample. Channeling effect at [001] zone axis of a crystalline sample can cause very small EDS signal. This can be avoided by slightly tilting the sample, whereupon the beam interacts with different atoms more efficiently, increasing the EDS signal.

5.4.3.8 Sample preparation

The preparation of high quality TEM samples is one of the most crucial steps for a microscopy investigation. The quality of the obtained results is fully dependent upon the quality of the sample. Properties like thickness, uniformity and cleanliness of the area of investigation constitute the limitations for a high resolution investigation of the sample in the TEM.

The requirement for sample thickness varies with different techniques, but the general rule is that thinner is almost always better. Electron transparency is crucial for transmission of the electron beam, therefore the specimen thickness shouldn't exceed a few hundred nanometers. To exclude effects like beam spreading within the sample

and plural scattering events, the specimen thickness should be kept below approximately one hundred nm.
Nowadays there are different methods available for preparation of very thin samples. A very famous one is using the modern lift-out technique, making use of a combined Focused Ion Beam and a Scanning Electron microscope (FIB/SEM).
Even though thickness is one of the primary considerations, it is even more important that the original properties of the sample are preserved during the preparation process.

In this thesis work, all the samples used for the investigations have been prepared with the so-called conventional sample preparation technique, to avoid the atomic structure from being altered. It has previously been shown that heavy ion bombardment would change the electrical properties of STO. The conventional sample preparation is a time consuming technique and requires a lot of patience. The technique is modeled in Fig. 21, and consists of cutting, gluing, polishing, grinding and precision Ar-ion milling.

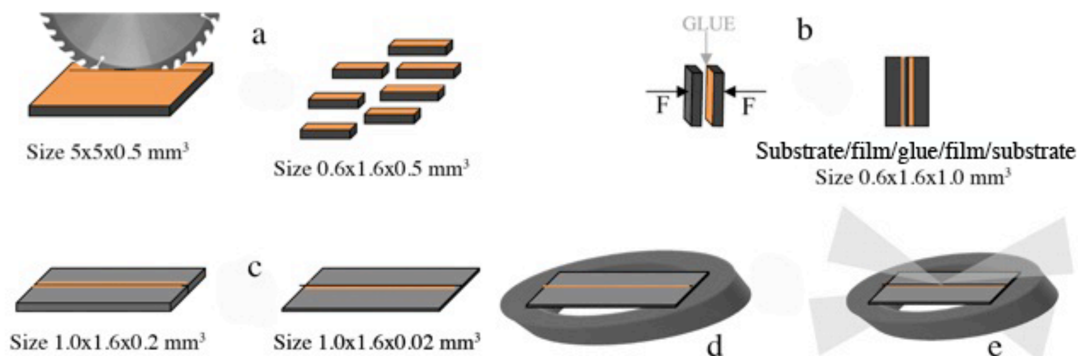

Figure 21: Conventional sample preparation technique:
5×5×0.5 mm sized samples are first cut into smaller pieces with a low speed saw.
Two equal sized smaller pieces are then glued together (using the epoxy M-bond), with the film surfaces facing towards each other.
The sample is ground and polished down to a thickness of around 20µm. For this a tripod is used which offers a high accuracy in controlling the thickness of the sample. In combination with diamond lapping films, it also gives a fast procedure and satisfying surface roughness.
After that the sample is glued to a titanium or molybdenum grid also using M-bond.
The sample is finally ion-milled until electron transparency is achieved, using the Gatan PIPS Ar ion mill [64].

The two most crucial steps for preparing the samples with the conventional method are gluing together two pieces, which will constitute the sandwiched sample, and the ion milling step. In order to obtain a good thin sample area still containing the thin film, we need as small and round hole as possible. To increase the chance to obtain such a result when ion milling, the glue line needs to be as thin as possible, because of the preferential ion-milling rate at the edges. This step requires high precision in cleaning the thin film surface and handling with the glue and the tweezers. The above mentioned along with the unpredictability of the ion-milling makes this step the most delicate procedure of this technique.

To investigate the quality of my samples I have been using the Philips CM200 FEG TEM with a Gatan energy filter to obtain thickness maps. Desired thickness is about 0.1 – 0.2 mean free paths.

6

Summary of appended papers

6.1 Paper I

The quasi-two dimensional electron gas formed at the interface between $LaAlO_3$ (LAO) and $SrTiO_3$ (STO) shows fascinating properties, such as two-dimensional superconductivity, giant electric field effect, and the possible co-existence of ferromagnetic and superconducting phases. In this work, we demonstrate that the conducting LAO/STO interface can be made insulating after short irradiation by a beam of low energy Ar+ ions. The irradiation process does neither result in physical removal of the LAO film nor produces oxygen vacancies in the STO layer. Using electron beam lithography and low ion beam energy irradiation, we fabricated conducting nano-structures in the LAO/STO interface with dimensions down to 50 nm. Such a reliable and robust method of nano-patterning may be a prerequisite for future electronic applications of the LAO/STO interface.

6.2 Paper II

We show a difference in microstructure between conducting and non-conducting interfaces of $LaAlO_3$ (LAO)/$SrTiO_3$ (STO). The microstructure was studied using high resolution analytical transmission electron microscopy (TEM) on cross-sectional samples. Both imaging and spectroscopy were used to compare the atomic structure of the two types of interfaces. The LAO/STO interfaces having a quasi-two

dimensional electron gas were patterned using argon ion beam irradiation and parallel lines of conducting (not exposed to the argon ions) and non-conducting (irradiated by the argon ions) were both electrically and structurally characterized. Our results show that the difference in conductivity is related to a change in composition of the LAO film where the La/Ti is 1.2 in the irradiated non-conducting lines while it is 1.0 in the conducting lines.

6.3 Paper III

The observation of a high-mobility two-dimensional electron gas between two insulating complex oxides, especially $LaAlO_3/SrTiO_3$, has enhanced the potential of oxides for electronics. The occurrence of this conductivity is believed to be driven by polarization discontinuity, leading to an electronic reconstruction. In this scenario, the crystal orientation has an important role and no conductivity would be expected, for example, for the interface between $LaAlO_3$ and (110)-oriented $SrTiO_3$, which should not have a polarization discontinuity. Here we report the observation of unexpected conductivity at the $LaAlO_3/SrTiO_3$ interface prepared on (110)-oriented $SrTiO_3$, with a $LaAlO_3$-layer thickness-dependent metal-insulator transition. Density functional theory calculation reveals that electronic reconstruction, and thus conductivity, is still possible at this (110) interface by considering the energetically favorable (110) interface structure, that is, buckled TiO_2/LaO, in which the polarization discontinuity is still present. The conductivity was further found to be strongly anisotropic along the different crystallographic directions with potential for anisotropic superconductivity and magnetism, leading to possible new physics and applications.

6.4 Paper IV

In this work we investigate 25 nm thick YSZ films, grown by pulsed laser deposition (PLD) on (001) $SrTiO_3$ (STO) substrates at low ($5x10^{-6}$ mbar) and high ($1x10^{-2}$ mbar) oxygen pressure. By using transmission electron microscopy we find characteristic surface morphologies and crystal orientations depending on the oxygen pressure during film growth. Dense and atomically flat surfaces are achievable under the right conditions, providing a useful underlay when thermally stable thin film ionic conductors are necessary. The origin of the different crystallographic arrangements of YSZ on STO substrate is explained in terms of the thermodynamic approach, where the effects of oxygen site configuration at the interface, as well as growth dynamics are addressed. We find that the oxygen pressure can be used to control the surface morphology on the atomic scale.

6.5 Paper V

In this work we address the effect of lattice match and growth characteristics on the microstructure, which can be very important for properties of YSZ films. 25 nm thick Yttrium-stabilized ZrO_2 (YSZ) films were deposited by pulsed laser deposition on (001) $SrTiO_3$ (STO) and (001) $LaAlO_3$ (LAO) single crystals. High-resolution transmission electron microscopy shows that the YSZ films are textured and smooth with different crystallographic orientations on the different substrates where STO has a larger unit cell and better lattice match compared to LAO. The relation between interface misfit and crystallographic orientation is made and discussed in terms of interfacial energy effects.

Acknowledgments

I would like to express my greatest gratitude to all the people who were involved in different ways in the process of making this work possible.

First of all thanks to my dear family, for always being there for me. It wouldn't be possible without your support.
My husband, for all the support and understanding through better and worse during these years. Not least for illimitable patience through some rougher times. A small thanks to a family member to come as well, for making me aware of a bigger perspective through the final period.

My supervisor Eva Olsson for providing this opportunity and for guidance and instructive experience through it.
My assistant-supervisor Alexey Kalabukhov for a very nice collaboration, with constantly fruitful discussions and providing all the necessary material. I would also like to acknowledge other collaborators from MC2 and Chemistry; Pier Paolo, Tord, Dag, Robert, Chris, Sam, Francis, Habib, for interesting and fruitful discussions and for your valuable inputs.
My other assistant-supervisor and friend Stefan Gustafsson, who with his constant flow of inspiration always finds the right thing to say. Thanks a lot for your help and support and especially for your unconventional ideas.

Thanks to all my former colleagues at Nanofactory Instruments for a pleasant and joyful working environment, especially Johan Angenete and Alexandra Nafari for providing a good learning experience and a nice start.

To all my colleagues in former Microscopy & Microanalysis, as well as the new ones: Luciana, Stefan, Henrik, Pia, Jenny, Haiping, Anna, Pavleta, Anke,… and all the others! Thank you all for providing a great atmosphere and for all your help, caring and kindness.
Many thanks to Anders and Ola for the technical support and Birgitta, Linda and Josephine for the administrative support.
Thanks to my former officemate Johan B. for providing a nice starting environment in the M&M group, as well as for sharing all the knowledge and support I needed for starting in this project.
Lunjie Zeng, I could not wish for a better officemate. Besides the kind help and support with both discussions and microscopy, thank you for putting up with occasional intense "Honeyness" that was going on in your close environment.
I can only be grateful for having the luck to have shared office with such great people.
Samirajun, Honey, what can I say... through all this time you have probably been the biggest support. Going through everything together, made the rough times easier and

the good once even better. Constant source of happiness. I will never forget all of our fun trips and may there be many more to come.

Bibliography:

[1] Bednorz J. G. and K. A. Muller, Zeitschrift fur Physik B Condensed Matter **64**, 2:189-193 (1986)

[2] Busch G. and P. Scherrer, Naturwissenschaften **23**, 43:737 (1935)

[3] Matthews J. W. and A. E. Blakeslee, Journal of Crystal Growth **27**(0):118-125 (1974)

[4] Goniakowski, J., F. Finocchi, et al., Reports on Progress in Physics(1): 016501 (2008)

[5] Jahn, H. A. and E. Teller, Proceedings of the Royal Society of London. Series A - Mathematical and Physical Sciences **161**(905): 220-235. (1937)

[6] Müller, K. A. and H. Burkard, Physical Review B **19**(7): 3593-3602 (1979)

[7] Noland, J. A., Physical Review **94**(3) (1954)

[8] Capizzi, M. and A. Frova, Physical Review Letters **25**(18): 1298-1302. (1970).

[9] Abramov Y. A., V. G. T., V. E. Zavodnik, et al., Acta Cryst. **B51**: 942-951 (1995)

[10] Okazaki, A. and M. Kawaminami, Materials Research Bulletin **8**(5): 545-550 (1973)

[11]Koster, G., B. L. Kropman, et al., Materials Science and Engineering: B **56**(2-3): 209-212 (1983)

[12] Schooley, J. F., W. R. Hosler, et al., Physical Review Letters **12**(17): 474 (1964)

[13] Tufte, O. N. and P. W. Chapman, Physical Review **155**(3): 796 (1967)

[14] Frederikse, H. P. R., W. R. Thurber, et al., Physical Review **134**(2A): A442 (1964)

[15] Koonce, C. S., M. L. Cohen, et al., Physical Review **163**(2): 380 (1967)

[16] Muller, D. A., N. Nakagawa, et al., Nature **430**: 657-661 (2004)

[17] Ohtomo A. and H. Y. Hwang, Nature **427** (2004)

[18] Nakagawa, N., H. Y. Hwang, et al. Nature Materials **5**(3): 204-209 (2006)

[19] Brinkman, A., M. Huijben, et al., Nature Materials **6**(7): 493-496 (2007)

[20] Kalabukhov, A., R. Gunnarsson, et al., Physical Review B **75**(12): 121404 (2007)

[21] Siemons, W., G. Koster, et al., Physical Review Letters **98**(19): 196802 (2007)

[22] Chen, Y., N. Pryds, et al., Nano Letters **11**(9): 3774-3778 (2011).

[23] Willmott, P. R., S. A. Pauli, et al., Physical Review Letters **99**(15): 155502 (2007)

[24] A. S. Kalabukhov, Y. A. Boikov, et al., PRL **103**(14):146101 (2009)

[25] Thiel, S., G. Hammerl, et al., Science **313**(5795): 1942-1945 (2006)

[26] Pauli, S. A. and P. R. Willmott, Journal of Physics: Condensed Matter **20**(26): 264012-264019 (2008)

[27] Kalabukhov, A. and et al., Journal of Physics: Conference Series **100**(8): 082039 (2008).

[28] Zhicheng, Z., P. X. Xu, et al., Physical Review B (Condensed Matter and Materials Physics) **82** 165127 (165125 pp.) (2010)

[29] G. Herranz, M. B., M. Bibes, Physical Review Letters **98** (2007)

[30] Basletic, M., J. L. Maurice, et al. Nature Materials **7**(8): 621-625 (2008)

[31] Reyren N., S. G., A. D. Caviglia, et al. Applied Physics Letters **94**(11):3 (2009).

[32] Copie O., V. G., C. Bödefeld, et al. Phys. Rev. Lett **102**(216804) (2009)

[33] Sing, M., G. Berner, et al., Physical Review Letters **102**(17): 176805 (2009)

[34] Scott, H. G., Journal of Materials Science **10**(9): 1527-1535 (1975)

[35] Yashima, M., M. Kakihana, et al., Solid State Ionics **86,**Äì88, Part 2(0): 1131-1149 (1996)

[36] Dixon, J. M., L. D. Lagrange, et al., Journal of the Electrochemical Society **110**(4): 276-280 (1963)

[37] Strickler, D. W. and W. G. Carlson, Journal of the American Ceramic Society **47**(3): 122-127 (1964).

[38] Gibson, I. R., G. P. Dransfield, et al., Journal of the European Ceramic Society **18**(6): 661-667 (1998).

[39] Kosacki, I., C. M. Rouleau, et al., Solid State Ionics, Diffusion & Reactions **176**(13-14): 1319-1326 (2005)

[40] Korte, C., A. Peters, et al., Physical Chemistry Chemical Physics **10**(31): 4623-4635 (2008)

[41] Sillassen, M., P. Eklund, et al., Advanced Functional Materials **20**(13): 2071-2076 (2010)

[42] Garcia, B., A. Rivera-Calzada, et al., Science **321**(5889): 676-680 (2008)

[43] Cavallaro, A., M. Burriel, et al., Solid State Ionics, Diffusion & Reactions **181**(13-14): 592-601 (2010)

[44] Pennycook, T. J., M. P. Oxley, et al., European Physical Journal, Applied Physics **54**(3): 33507 (33511 pp.) (2011)

[45] Cavallaro, A., B. Ballesteros, et al., CrystEngComm **13**(5): 1625-1631 (2011)

[46] Hidalgo, H., E. Reguzina, et al., Surface and Coatings Technology **205**(19): 4495-4499 (2011)

[47] Infortuna, A., A. S. Harvey, et al., Advanced Functional Materials **18**(1): 127-135 (2008).

[48] Heiroth, S., T. Lippert, et al., Applied Physics A: Materials Science & Processing **93**(3): 639-643 (2008)

[49] Shin, J., P. Li, et al. Thin Solid Films **517**(2): 648-651 (2008)

[50] Flamini, C., A. Giardini Guidoni, et al., Applied Surface Science **138**,139(0): 344-349 (1999)

[51] Pentcheva R. and W. E. Pickett, Physical Review B **78**(20):205106 (2008)

[52] Savoia, A., D. Paparo et al., Physical Review B **80**(7):075110 (2009)

[53] Park M. S., S. H. Rhim et al., Physical Review B **74**(20):205416 (2006)

[54] Chambers S. A., M. H. Engelhard et al., Surface Science Reports 65(10-12):317-52 (2010)

[55] Jia C. L., S. B. Mi, et al., Physical review B **79**(8):081405

[56] Tuller, H. L., Solid State Ionics **131**(1): 143-157 (2000)

[57] Lubomirsky, I., J. Fleig, et al., Journal of Applied Physics **92**(11): 6819-6827 (2002)

[58] Maier, J., Zeitschrift fur Physikalische Chemie **21**7(4): 415-436 (2003)

[59] Maier, J., 14th International Conference on Solid State Ionics (SSI-14), 2003, Netherlands, Elsevier (2004)

[60] Schichtel, N., C. Korte, et al, Physical Chemistry Chemical Physics **11**(17): 3043-3048 (2009)

[61] Gunnarsson, R., A. S. Kalabukhov, et al., Surface Science **603**(1): 151-157 (2009)

[62] Gunnarsson, R., "PHD Thesis" Chalmers University of Technology (2004)

[63] Williams, D. B. and C. B. Carter, New York, Plenum Press (1996)

[64] Börjesson J. PhD thesis, Chalmers University of Technology (2009)

[65] Haider M., H. Rose et al., Ultramicroscopy 75(1):53-60 (1998)

[66] Haider M., S. Uhlemann et al. Nature 392(6678):768-769 (1998)

[67] Jia, C. L., M. Lentzen, et al., Microscopy and Microanalysis 10:174-184 (2004)

[68] Nellist P. D., M. F. Chisholm et al., Science 305(5691):1741 (2004)

[69] Pennycook, S. J. SPIE 1284 (1990)

[70] Oxley M. P., S. J. Pennycook (1991)

[71] Mkhoyan, K. A., S. E. Maccagnano-Zacher, et al., Ultramicroscopy **108**: 791-803 (2008).

[72] Haruta, M., H. Kurata, et al., Ultramicroscopy 109(4): 361-367 (2009)

[73] Oxley, M. P., M. Varela, et al., Physical Review B **76**(6): 064303 (2007)

[74] Hillyard, S. and J. Silcox, Ultramicroscopy **52**(3): 325-334 (1993)

[75] Pennycook, S. J. and D. E. Jesson, Ultramicroscopy **37**(1-4): 14-38 (1991).

[76] Mkhoyan, K. A., S. E. Maccagnano-Zacher, et al., Ultramicroscopy **108**:791-803 (2008)